Understanding Non-Photochemical Laser Induced Nucleation

Sanjana Dhingra

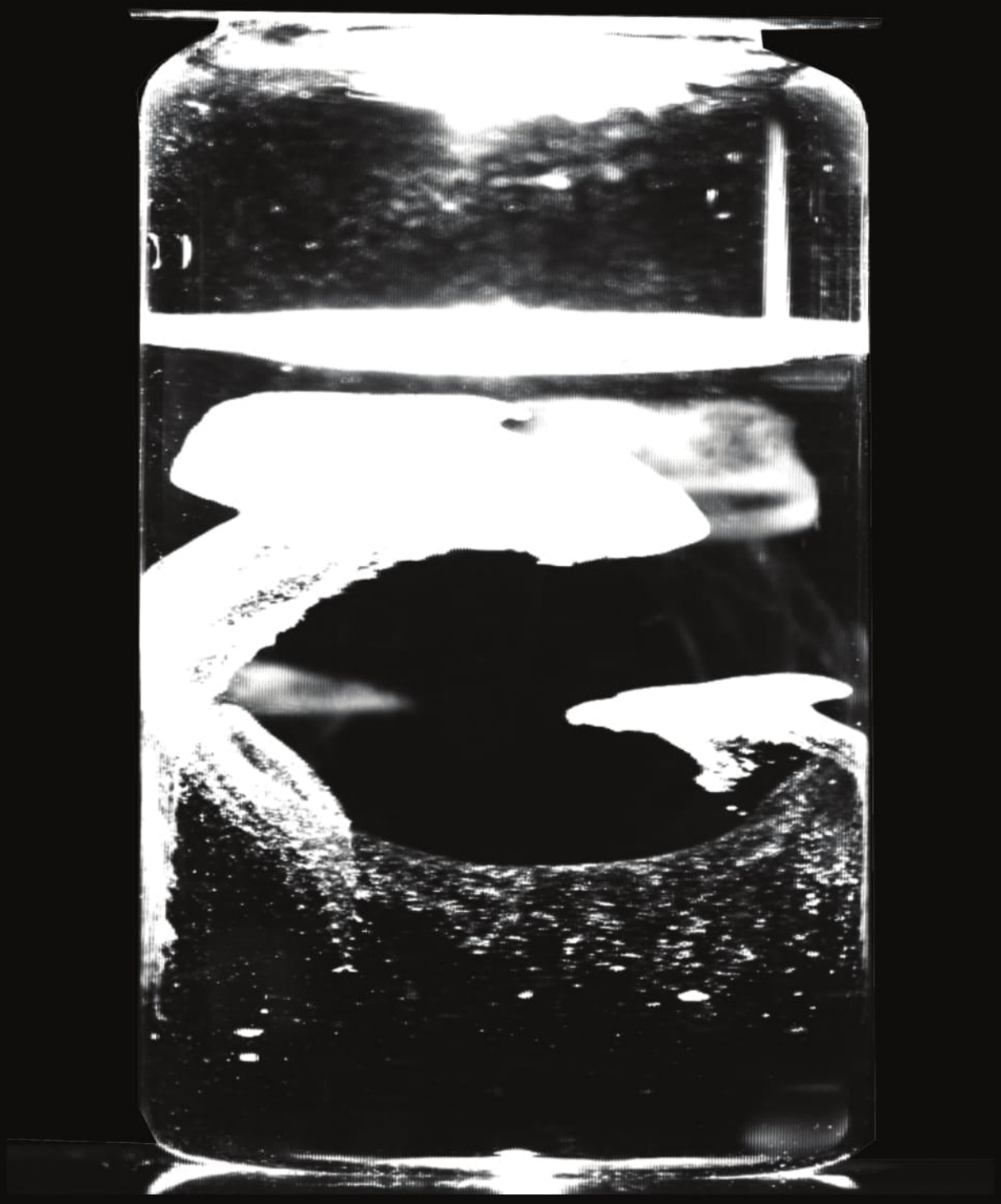

TU Delft
Delft University of Technology

Challenge the future

Understanding Non-Photochemical Laser Induced Nucleation

by

Sanjana Dhingra
4520475

in partial fulfillment of the requirements for the degree of

Master of Science

in Chemical Engineering

at the Delft University of Technology,

to be defended publicly on Thursday August 17, 2017 at 13:00 hours.

Under Guidance and Supervision of :	dr. Daniel Irimia,	TU Delft
	ir. Rohit Kacker,	TU Delft
	dr. ir. Herman J. M. Kramer,	TU Delft
	dr. H. B. Eral,	TU Delft
Thesis committee:	dr. H. B. Eral,	TU Delft
	Prof. dr. Antoine van der Heijden,	TU Delft
	Prof. em. Johan Grievink,	TU Delft

Front cover image represents a cloud of powdered KCl crystals forming in its aqueous supersaturated solution on laser exposure. Image credits: Sanjana Dhingra, ir. Rohit Kacker & dr. Daniel Irimia.

TU Delft Delft University of Technology

Abstract

Nucleation is the initial step for the creation of a new crystalline phase. A precise control over nucleation and its kinetics is important for both research and industries. Thus, alternative methods are sought after to extend the toolbox for understanding and controlling nucleation. In the 1990's, Non-Photochemical Laser Induced Nucleation (NPLIN) was suggested as a promising method to alter the nucleation kinetics. Since then, several reports have demonstrated that NPLIN dramatically reduces the nucleation induction time and controls polymorphism of various fine chemicals relevant to the industrial practice. Although different hypotheses have been proposed in the literature to explain the experimental observations, the mechanism behind NPLIN is still unknown.

The objective of this work is to extend the mechanistic understanding of NPLIN. This has been approached by quantitatively studying the effect of different factors on the nucleation efficiency of the non-photochemical process using unfocused pulsed laser in aqueous supersaturated solution of KCl. The factors investigated include wavelength, peak intensity, supersaturation, mixing, and impurity level of the solution. Each of these parameters are studied using a large number of samples (80-100) to generate a robust set of results and to avoid the stochastic nature of nucleation.

An acoustic wave was detected in the solution due to the interaction of the unfocused laser with the system by measuring the pressure signal with a piezo-electric transducer placed just below the air-liquid interface. Further experiments were executed to understand the nature of the acoustic wave and its influence on NPLIN. The results show that laser could induce nucleation at significantly low peak intensities, much below the previously reported intensity threshold in literature. It is also observed that NPLIN shows a strong dependence on peak intensity, supersaturation, impurity level, and mixing of the solution while the dependence on wavelength was found to be weak. Furthermore, the acoustic wave experiments show that the laser induced pressure fluctuations do not affect the nucleation efficiency of the process. Overall, the results suggest that several mechanisms play a role during laser induced nucleation. To summarize, the research provides a robust analysis of different factors that can influence NPLIN. The results can be further utilized to enhance the understanding and applicability of the process.

Contents

List of Figures

1

Introduction

Crystallization involves nucleation of the crystal and its subsequent growth. Since nucleation of the crystal forms the heart of the process, this makes it crucial to understand and control it. Different techniques such as sonocrystallization, microwave assisted nucleation control, electric field, and magnetic field induced nucleation have been demonstrated to provide a better control over nucleation than the traditional techniques [1–7]. After its accidental discovery in 1990's, Non-Photochemical Laser Induced Nucleation, usually referred to as NPLIN, has also been demonstrated as a promising alternative method to enhance nucleation kinetics and polymorphism control [8, 9]. This chapter provides a brief theoretical insight to nucleation and NPLIN followed by the objectives of this thesis.

1.1. Theoretical Background of Nucleation

Nucleation refers to the process of self-organization of the solute particles to form a new thermodynamically stable phase. This "birth" of crystal from the solution requires a precondition of the state of supersaturation in the solution. Supersaturated solutions have an excess concentration of the solute than the equilibrium concentration, so the supersaturation acts as a driving force for the solutions to attain equilibrium via crystallization. For practical applications, the degree of supersaturation of a solution is formulated in different ways. In this study, it is defined by the means of supersaturation ratio. The supersaturation ratio, S, is a dimensionless quantity and is expressed as the ratio of the solution concentration (c) to the equilibrium concentration (c^*) at a given temperature (T).

$$S(T) = \frac{c}{c*} \tag{1.1}$$

The supersaturated solutions can be further related to the susceptibility of the system to nucleate by segmenting the solubility diagram into three different zones (figure 1.1). The stable zone is bounded by the equilibrium line. The solutions in this zone are undersaturated and nucleation is unfeasible. Solutions in both the metastable and labile zone are supersaturated but in the metastable zone occurence of spontaneous nucleation is improbable. In the metastable zone, crystal growth takes place on introducing an external crystalline surface into the solution whereas in the labile zone uncontrolled spontaneous nucleation occurs in the system. The boundary demarcating the labile and the metastable zone and the width of the metastable zone is ill-defined because it can be altered by various different factors including agitation rate, cooling rate, impurities, volume of the solution, etc [11, 12]. Nevertheless, determination of metastable zone width (MSZW) is important for both industrial and research applications as MSZW describes the operating zone for most of the crystallization processes.

The flowchart in figure 1.2 represents the different nucleation mechanisms. NPLIN deals with inducing primary nucleation in the system. Primary nucleation, in contrast to secondary nucleation,

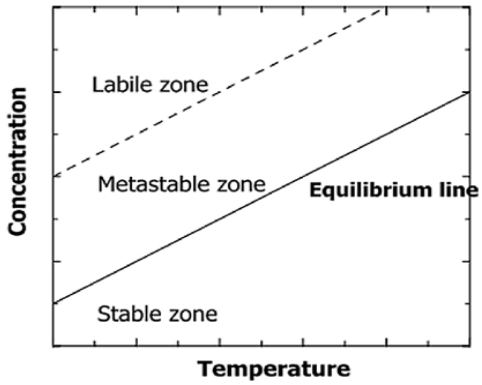

Figure 1.1: Solubility diagram showing three different zones for nucleation [10].

refers to the induction of nuclei in absence of any other solute crystals. Primary nucleation can be further classified into homogeneous and heterogeneous nucleation. Homogeneous nucleation, unlike heterogeneous nucleation, occurs in the absence of any impurities and in practice only occurs in highly supersaturated ultra-pure systems [13]. Despite the importance of crystal nucleation, the fundamentals

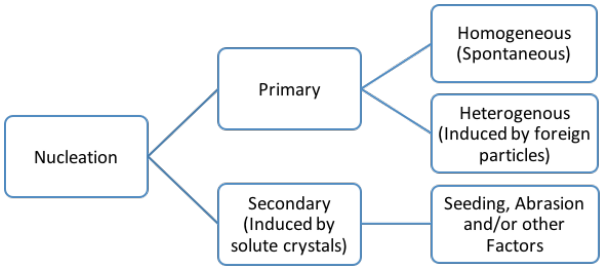

Figure 1.2: Classification of different nucleation mechanisms [13].

of nucleation are still not well-understood as a consequence of the inaccessible spatial and temporal scales of the event. The two widely applied nucleation theories are the Classical Nucleation Theory (CNT) and the two-step nucleation theory. CNT is the oldest and the simplest nucleation theory. This theory assumes that clusters of the solute molecules are formed in a supersaturated solution by the addition mechanism until the cluster achieves a critical size and becomes a stable nucleus. According to this theory, size of the critical nuclei in the metastable zone depends on an overall compensation between the surface energy gain due to formation of a solid-liquid interface and the solution's chemical potential reduction due to phase transformation. According to CNT, nucleation is one step process where density fluctuations and ordering of the solute molecules occur simultaneously. On the other hand, as the name suggests, two-step nucleation theory is a multiple barrier process in which the first barrier is the cluster formation due to density fluctuations and the second barrier is the transformation of cluster into an ordered crystalline structure [14, 15]. This theory is relatively modern and has been theoretically and experimentally validated for short-range interacting molecules such as proteins [16, 17]. However this theory requires further extensive investigation in order to extend it to other liquid-solid equilibrium systems. Although the fundamental theory underlying nucleation is still inconclusive, nevertheless the necessary requirement of exceeding a thermodynamic potential is evident in both the theories. Also, the dependence of nucleation on the random thermal and density fluctuations to produce pre-nucleating solute clusters induces the characteristic of stochasticity to the process of nucleation.

1.2. Non-Photochemical Laser Induced Nucleation

Almost two decades ago, NPLIN was discovered accidentally by Garetz *et al.* while studying the non-linear optical properties of supersaturated aqueous solutions of urea. It was reported that nanosecond

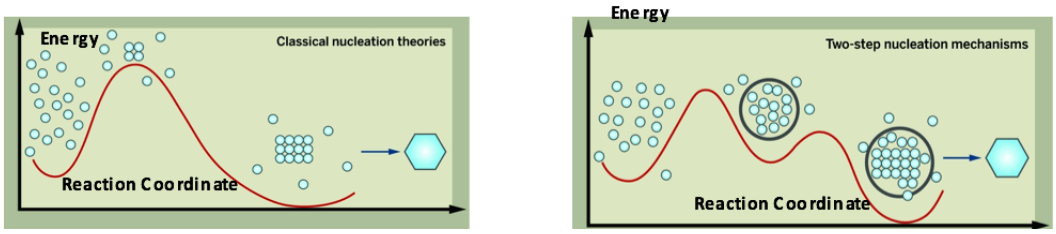

Figure 1.3: Different pathways of nucleation suggested by Classical Nucleation Theory and Two-step nucleation theory, respectively.

pulses of near infrared light (1064 nm) could drastically reduce the induction time of urea crystals up to an order of O^6 minutes and control the alignment of the crystal through polarization of the incident beam [8]. The transparency of the supersaturated solutions to the incident light distinguishes it from the well-understood phenomena of nucleation induction from photochemical reaction mechanism. Since its emergence, several reports point out the successful demonstration of NPLIN on other chemical compounds such as glycine, *L*-histidine, hen egg white protein, KCL, sulfathiazole,etc in different solvents such as water, ethanol and agarose gel [9, 18–21]. Besides these successful demonstrations on widely varying solute-solvent systems, the principle mechanism behind NPLIN is not well-understood. Following sub-sections briefly describe the different mechanisms reported in the literature.

1.2.1. Optical-Kerr Effect (OKE)

Optical-Kerr effect (OKE) was first suggested by Garetz and co-workers to explain the induction of needle-like crystal of urea and its subsequent alignment along the polarization of the incident monochromatic beam [8]. It was hypothesized that the principle mechanism of NPLIN was dependent on the interaction of the oscillating electric field of the incident beam with the pre-nucleating clusters in the supersaturated solution. The electric field can induce dipole in the system and further produce a torque to align the anisotropic polarization axis of the molecules in the cluster along the field direction and thus accelerating the structural ordering of the cluster to form a crystal (or reducing the second activation barrier according to two-step nucleation theory). This hypothesis was further strengthened by the demonstration of the so-called phenomena of 'Polarization Switching'. It refers to the induction of different polymorphs or different crystal structure of the chemical compound depending on the polarization of the incident laser beam [9]. For a specific range of supersaturation, it was reported that a linearly polarized light could induce the less stable γ form of glycine in the solution while the circularly polarized light induced α glycine in the solution [9, 22]. A similar phenomena was observed for supersaturated solutions of L-histidine [18].

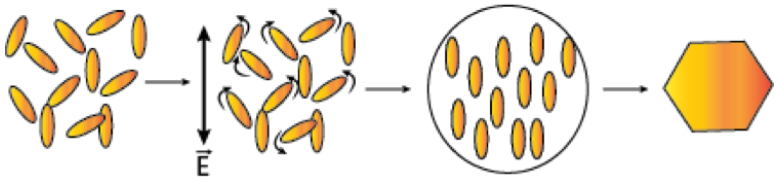

Figure 1.4: Schematics of the OKE hypothesis which proposes the enhancement of ordering of solute molecules in pre-nucleating clusters due to interaction of electric field of laser and induced dipole in the system leading to formation of crystal.

In a further attempt to support the hypothesis, crystals of glycine were induced in its aqueous supersaturated solution using dc electric field with an equivalent electric field strength of laser beam [23]. However, the major drawback of this hypothesis is that the interaction energy between the incident electric field and the induced dipole is orders of magnitude too low for the employed laser intensities [22]. This implies that the torque produced is too low to account for the observed decrease in activation energy for nucleation. A Monte Carlo simulations study by Knott and co-workers also

concludes that the orientation produced by the electric field of the laser fails to reduce the activation energy of the process significantly [24].

1.2.2. Isotropic Electronic Polarization

The mechanism of electronic polarization was suggested by Alexander and co-workers after observing the induction of single KCl crystal using single pulse of 1064 nm light at laser peak intensities much lower than that reported by Garetz *et al.* [20]. The mechanism of OKE was excluded because KCl crystals lack a preferable polarization axis. Hence, an alternative hypothesis of isotropic electronic polarization of the pre-nucleating cluster was proposed.

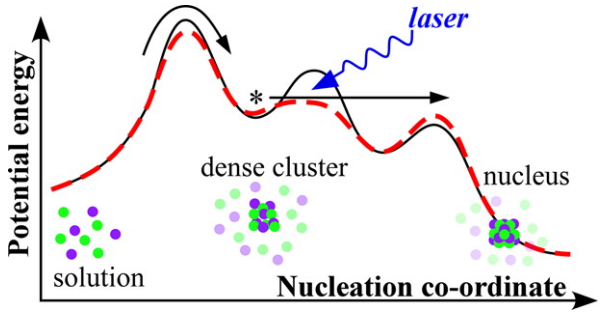

Figure 1.5: The schematics of isotropic electronic polarization as suggested by Ward *et al.* showing the decrease in activation energy barrier of the pre-nucleating crystal due to dielectric effects arising from the electric field of laser [25].

Electronic polarization refers to the shifting of electronic cloud around a positive nucleus in response to an external electric field. Since the relaxation time for electronic polarization is $\sim 10^{-15}$ s, this polarization mechanism can be considered as an instantaneous response to the oscillating frequency of the electric field ($\sim 10^{14}$ Hz) of the laser beam. The hypothesis proposed by Alexander and co-workers is established on the fact that the free energy of a dielectric particle is reduced when it is immersed in a medium of comparatively lower electric permittivity [26]. This reduction in free energy of the pre-nucleating clusters leads to reduction in the size of critical nuclei and thus enhancing the nucleation kinetics. The hypothesis is further supported by analyzing the experimental results using a model which includes the dielectric free energy change in the classical nucleation theory. However, in the published study an empirical scaling factor of magnitude $\sim 10^4$ is used to fit the experimental data which acts as a major weakness to the accountability of the hypothesis. The hypothesis also fails to explain the dependence of NPLIN on the polarization of the light.

1.2.3. Heating of Nano-Impurities

In addition to nucleation of solid crystals in a liquid medium, laser has also been reported to induce bubbles in a supersaturated system. The phenomena of laser induced bubble nucleation was first reported by Brandon and co-workers in 2011 [27]. It was reported that the transient bubbles of CO_2 were induced in a supersaturated aqueous carbonated solution on exposing the solution to multiple pulses of light of different wavelengths (355, 532 and 1064 nm). In the same study, through a different series of experiment, they further show that the generation of argon bubbles in a supersaturated solution of glycine was enough to induce crystallization of glycine. The above set of observations were combined to suggest a mechanism which involves the generation of small sized transient bubbles on exposing the solution to laser which can further accelerate the crystal nucleation.

In a more recent work by Martin *et al.*, a similar observation of induction of CO_2 bubbles is reported [28]. Additionally, it was learned that filtering of the solutions prior to the laser exposure lead to decrease in the number of bubbles induced. The study suggests a hypothesis of absorption of light by the nanoparticles existing in the system in the forms of molecular impurities (intrinsic) and/or dust particles (extrinsic). The nanoparticles are assumed to heat up on absorbing the incident light and the resulting heat is then assumed to be transferred adiabatically to the surrounding liquid to vaporize a shell of liquid around the particles. It is suggested that growth of these vapor bubbles can promote

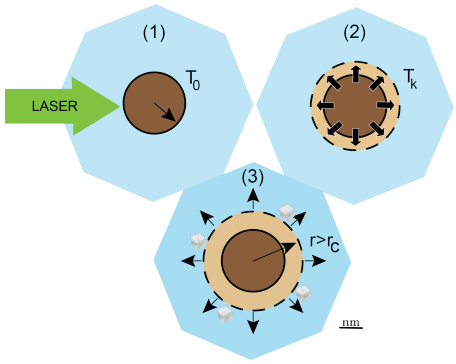

Figure 1.6: Schematics of the hypothesis suggesting absorption of laser by the nano-particles followed by transferring of heat to vaporize a shell of liquid around the impurity leading to nucleation of crystals on the growing vapor bubble. Adapted from Martin *et al.* [28].

aggregation and accumulation of the solute molecules at the vapor-liquid interface which drives them to nucleate and form crystals. Due to inaccessible spatial scales of this mechanism, acquiring a visual evidence for this hypothesis is difficult and complex.

1.2.4. Laser induced Soundwave assisted Crystallization

In a study by Nasrin and co-workers, it was learned that the laser pulses of 1064 nm when focused into a solution were capable of producing pressure gradients in the solution [29]. Compression waves were generated in solutions both when the laser was directly and indirectly focused in to the solution. Crystals were formed in the bulk volume of the solution (instead of forming near the focal point of laser) which indirectly confirmed the induction of crystallization due to the generated pressure fluctuations. The variation of the local pressure and temperature due to the travelling of pressure wave through the solution was reasoned to alter the nucleation kinetics by influencing the chemical potential of the system which acts as the driving potential for nucleation. The experiment was demonstrated on aqueous supersaturated solution of different chemical compounds (sodium borate, sodium chloride and tartaric acid). The figure 1.7 shows the schematics of generation of the pressure waves and consequent induction of NaCl crystals from the indirect interaction of the focused laser beam and the supersaturated solution. Since the laser beam was focused for these experiments, the incident laser peak intensities were larger than that reported in earlier studies of NPLIN $(O(10^6))$.

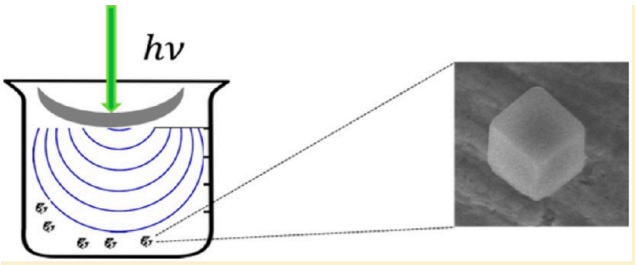

Figure 1.7: In the work of Nasrin *et al.*, the laser beam was focused on a metal boat to generate pressure fluctuations in the aqueous supersaturated solution of NaCl to induce its crystals [29].

1.3. Thesis Objectives

The objective of this thesis is to enhance the understanding of laser induced nucleation. The research involves study of NPLIN in aqueous supersaturated solutions of KCl. Different factors related to the characteristics of the laser beam, process conditions and hydrodynamics of the solution have been studied. The following tasks were executed during the course of this thesis:

- Determination of the meta-stable zone width of KCl and its UV-VIS absorption spectrum.
- Designing an optical set-up and experimental scheme for successful implementation of the experiments.
- Analyzing the effect of different factors on the nucleation efficiency of NPLIN. The factors considered in this thesis are peak intensity and wavelength of laser, supersaturation, level of impurities, and mixing of the solution.

Additionally, a transient pressure wave was recorded in the system on laser exposure. Further experiments were executed to understand the nature and origin of the pressure wave and its influence on NPLIN.

2

Comparative Analysis of NPLIN

In an attempt to get a better understanding of the mechanism behind NPLIN, it is necessary to study the different factors which might influence the nucleation ability due to laser. This chapter involves the study of influence of different factors on NPLIN which were found relevant to the existing hypothesis on mechanisms of NPLIN. The factors analyzed in this section are peak intensity and wavelength of the incident beam, supersaturation of solutions, effect of impurities, and mixing in the solution.

2.1. Materials and Methods

Supersaturated aqueous KCl solutions were used for dependency study of NPLIN. KCl (Sigma Aldrich, molecular biology ≥ 99.0%) was used without any further purification and the deionized water was obtained from an in-house dispenser (Elga PURELAB Ultra, 3.7 MΩ.cm). This section further contains the description of different equipment used and the experimental procedures implemented during different phases of the experiment.

2.1.1. Solubility and Meta-Stable Zone Width (MSZW) determination

In order to determine the operating supersaturation for the NPLIN experiments, it was necessary for the supersaturated solutions to be confined within the metastable zone of KCl. Metastable zone width measurements were performed using the Crystal 16 (Avantium) parallel crystallizer system. The integrated turbidity sensor in the system allowed to record the event of crystal formation and crystal nucleation by means of change in the laser transmissivity through the solution. Solutions of KCl (∼1 ml) with different concentrations were subjected to a user-defined heating-cooling cycles and the corresponding laser transmissivity was recorded. Figure 2.1 shows the image of the apparatus and an example of the temperature program and measured transmissivity data obtained from the equipment.

The observed temperature difference between the clear state (100% transmissivity) and cloud state (0% transmissivity) is termed as meta-stable zone width for the respective concentration. Such measurements are made for a range of concentrations to obtain the solubility data (clear points) and the cloud data (cloud points).

2.1.2. Absorption spectrum of aqueous KCl solution

To determine the experimental range for wavelength study, an experimental sample of KCl solution was analyzed in a double beam UV-VIS spectrophotometer (Hitachi U-2900). The spectrophotometer works on a simple principle of measuring attenuation of a light beam when the light passes from the

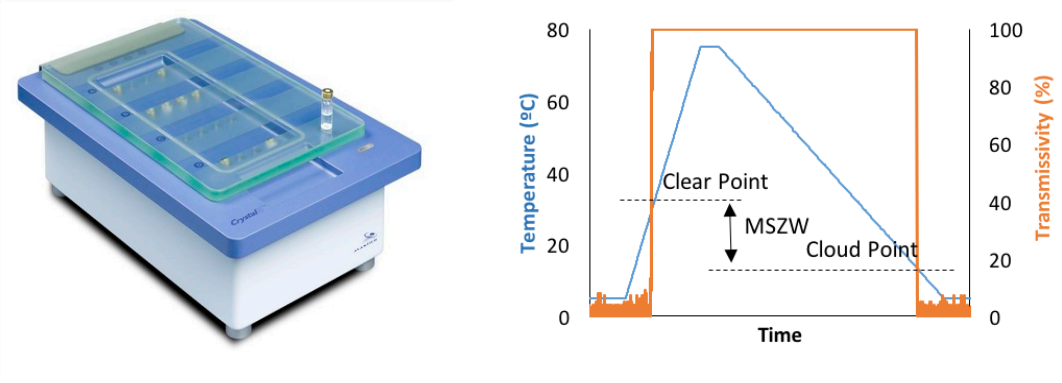

(a) (b)

Figure 2.1: (a) Parallel crystallizer apparatus (crystal 16) used for MSZW measurement and; (b) the graph exemplifies the technique to measure MSZW from the applied temperature program and the obtained tranmissivity data

sample. The KCl solution was analyzed for the spectral range of 200 nm to 1100 nm with a scanning rate of 200 nm min^{-1}. Figure 2.2 represents the image of the equipment.

Figure 2.2: Double beam UV spectrophotometer used to measure the absorption spectrum of aqueous KCl solution.

2.1.3. NPLIN of aqueous KCl solution

The execution of NPLIN experiments is categorized into two sections. The first one deals with the setting up of the optics for the laser beam and the second category deals with the scheme of sample preparation & testing.

- *Optical Set-up*: A Q-switched Nd:YAG laser (Continuum Powerlite DLS 8000 model) was used to generate a train of linearly polarized 7 ns light pulses at the repetition rate of 10 Hz and the fundamental wavelength of 1064 nm. The fundamental beam was further frequency doubled and tripled via second harmonic generation (SHG) and third harmonic generation (THG) processes in laser's nonlinear crystals to produce new wavelengths at 532 nm and 355 nm respectively. The output powers at the new wavelengths could be varied by gently changing the alignment of the KDP crystals and thus altering their SHG/THG conversion efficiencies. The laser beam was then passed through a self-assembled two lens telescope system to shrink the beam diameter from 9 mm to 4.5 mm. The energy of the light pulses was carefully measured before and after the sample vial (points 7 & 9 in figure 2.3) using a power/energy meter (Gentec Electro Optique-Maestro Monitor) while the pulse duration was precisely monitored with a high-speed photodetector (Thorlabs DET10A; 1 ns rise time). Figure 2.3 shows the schematic representation of the set up and the image of the experimental set up.

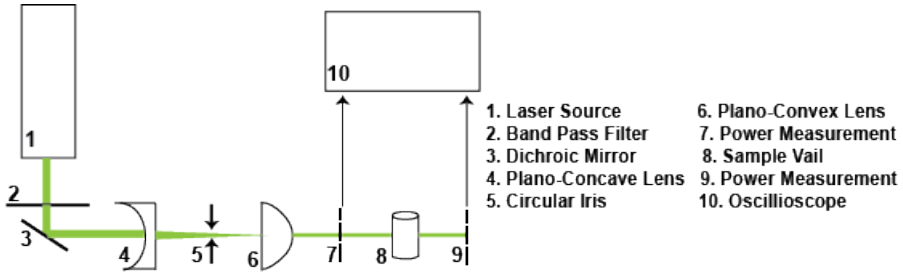

(a)

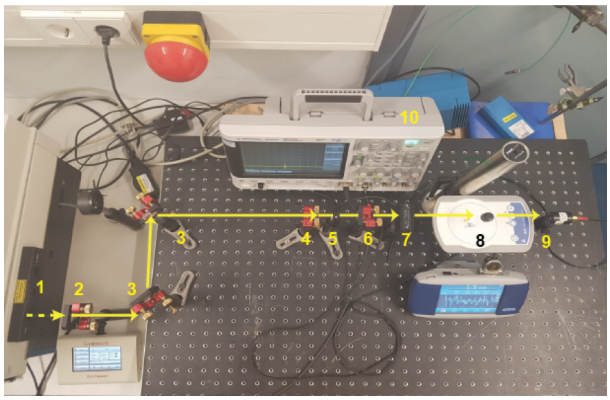

(b)

Figure 2.3: (a) Schematics of the optical setup showing the different components of the setup and the path of laser beam (b) Image of the experimental setup where the yellow line represents the ray path.

- *Sample Preparation & Testing*: Deionized water was added to analytically weighted KCl to achieve the desired concentration and the solution was heated at 50 °C for two hours. On dissolution of KCl in water, the heated solution was transferred to 1.3 cm borosilicate glass vials (8 ml). A set of 100 sample vials were prepared for each desired concentration. These vials were again heated overnight at 50 °C in an oven to ensure that all of the KCl is dissolved. Finally, the vials were cooled down to the room temperature (24±1°C) before exposing them to laser. Concentrations prepared in this way did not nucleate spontaneously and were stable for a period of 1-2 weeks. During every experiment, samples were exposed to a single pulse of laser. After the laser exposure, a maximum waiting period of 60 minutes was provided for each sample set to visually detect the crystals. Within the waiting period, the vials were evaluated manually after every 5 minutes to note the number of vials that showed crystals. Most of the factors were analyzed using 80-100 samples with an objective of producing a robust statistical data. However, the impact of impurities and mixing was analyzed using 10 samples.

2.2. Results

2.2.1. Solubility and Meta-Stable Zone Width (MSZW) Measurements

The measured data for clear and cloud points from crystal 16 was fitted with a linear trend line to obtain the solubility diagram and the MSZW of KCl which is shown in figure 2.4. At 24 °C, the saturation solubility of KCl was found to be 357.3 mg of KCl / mg of water with a MSZW of 55 mg of KCl / mg of water. The value of saturation solubility is in close agreement with the solubility value of 352.4 mg of KCl / mg of water published in [30]. The operating window for the experiments thus lies between 357.3 mg of KCl / mg of water and 412 mg of KCl / mg of water. Therefore, the prepared solutions had a concentration of 369 mg of KCl / mg of water and 377 mg of KCl / mg of water which accounts for supersaturation ratio of 1.035 and 1.055 at 24 °C, respectively. It should be noted that the experiments were executed at room temperature for which fluctuations of 24±1°C were observed causing an error

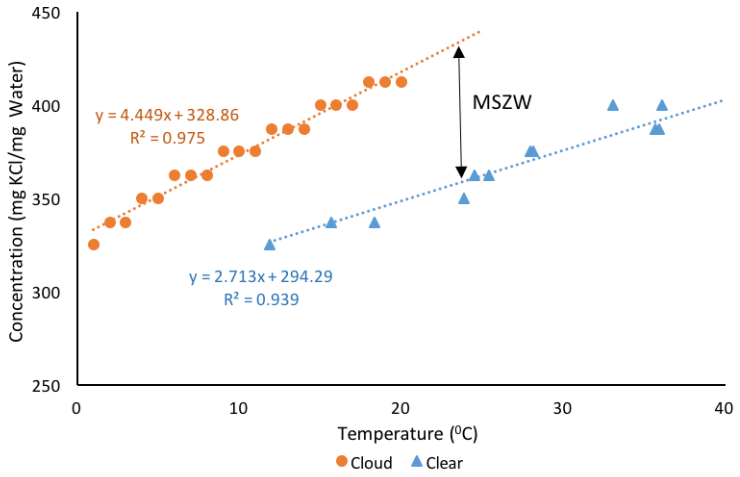

Figure 2.4: Solubility diagram of KCl obtained by fitting a linear trend line on the measured cloud and clear temperatures. The double arrow headed line represents the MSZW at 24 °C.

of ±2% in the supersaturation ratio. The fact that the prepared concentrations were enclosed in the MSZW aided in avoiding the spontaneous nucleation of KCl and ensured the induction of crystals from laser.

2.2.2. UV-VIS Spectrum of KCl Solution

Figure 2.5a depicts the absorption spectrum of the KCl solution sample with the supersaturation ratio of 1.035. A minor peak with apex at 269 nm is measured due to the absorbance of KCl alongwith a peak ranging from 920 nm to 1100 nm owing to the absorbance of water [31]. The inherent wavelengths from the laser are 355, 532 and 1064 nm. The solution is completely transparent to 355 and 532 nm. Due to the slight absorbance of 0.03 at 1064 nm, the consequent temperature increase of the solution is calculated to be very less (2.4×10^{-4} °C) at the maximum power output (1 W) of each laser pulse of 7 ns, and thus can be overlooked.

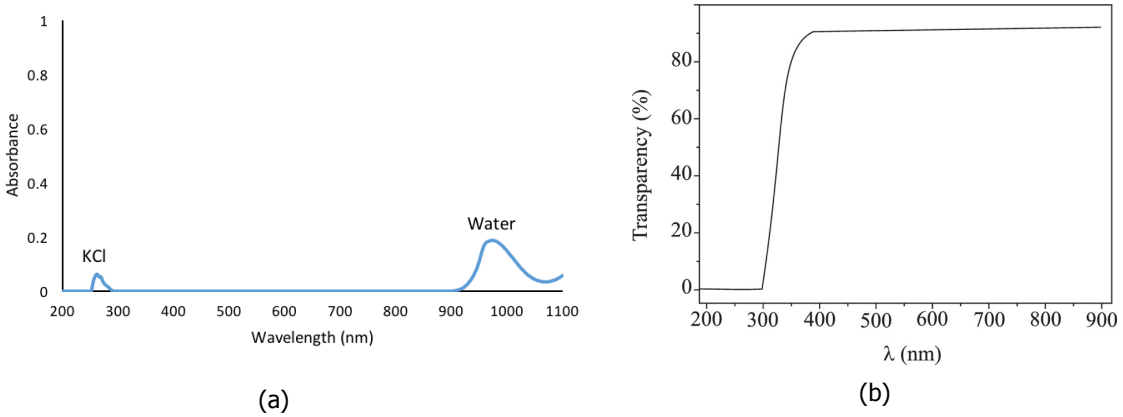

Figure 2.5: (a) Measured UV-VIS spectrum of KCl solution with S = 1.035 showing minor peaks with apex at 269 nm and 980 nm due to absorbance of KCl and water, respectively and; (b) Transparency of borosilicate glass for wavelength range of 190 nm to 900 nm showing the change in transparency of the glass below350 nm, approximately [32].

Since the KCl solutions were exposed to laser in the borosilicate glass vials, it is important to verify the material's transparency at the experimental wavelengths of 355, 532 and 1064 nm. Figure 2.5b represents the transparency of borosilicate glass as studied by Pejovic *et al.* [32]. The glass is highly transparent (91.2%) at wavelengths of 532 and 1064 nm but the transparency begins to drop below

350 nm. As a result for the experimental wavelength of 355 nm, the transparency is on the edge of the curve and partial absorption and reflections can be expected at this wavelength as compared to 532 and 1064 nm.

2.2.3. NPLIN of Aqueous KCl Solutions

During the experiments, some common observations were made concerning the NPLIN regardless of the incident wavelength of laser and the supersaturation of the solution. Firstly, the number of crystals formed on laser exposure were found to increase with the increase in the power input of the pulse while a single crystal was formed at low power intensities (<10 MW/cm^2) . The induced crystals exhibited different shapes. Secondly, on exposing the samples to more than one pulse of laser at high power intensities (>10 MW/cm^2), immediate showering of powder like crystals was observed. Thirdly, it was noted that the formation of the nuclei started along the path of the laser beam in the solution. The different images in the figure 2.6 capture the above mentioned observations.

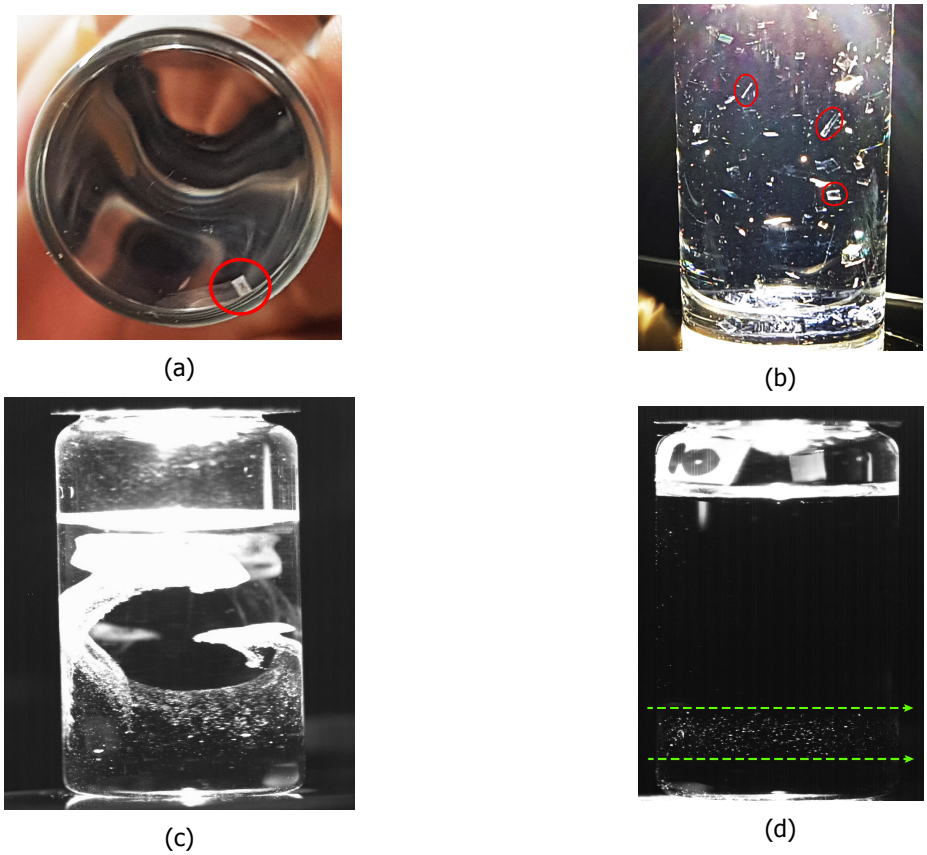

Figure 2.6: (a) Formation of single crystal on exposing the supersaturated solution (S = 1.055) to single pulse of laser of 532 nm at power intensity of 1 MW/cm^2; (b) Crystals falling in the solution (S = 1.055) after exposing it to a single pulse of laser of 532 nm at power intensity of 100 MW/cm^2. Circles highlight the different crystal habit induced in the system; (c) Cloud of powder like crystals formed in the solution on exposing the solution to multiple laser pulses (20) of power intensity 100 MW/cm^2; (d) Crystal formation starting along the path of the beam in the solution. The picture frame was acquired 7 s after exposing the solution to single pulse of 532 nm at the power intensity of 95 MW/cm^2. The green line represents the path of the laser.

Lastly, a common trend was observed for cumulative nucleation probability with respect to induction time of crystals as depicted in figure 2.7. In the context of this work, induction time refers to the time between laser exposure and manual observation of the crystals. Additionally, the cumulative nucleation probability for induction time, t, is defined as a ratio of number of samples that nucleate between the time zero and time t to the total number of samples that were exposed to laser at time zero. As cumulative probability distribution of induction time is suggestive of nucleation kinetics of a process, a trend regarding the kinetics of NPLIN can be established from figure 2.7 [33]. For high power

intensity of laser, the nucleation kinetics is faster than the kinetics at low power intensities. The steep increase in the nucleation probability is followed by a relatively slower increase, and finally a stagnant period, where no more nucleation takes place. This effect of peak intensity on the induction time was consistent irrespective of the incident wavelength. Due to the limitations of manual observation, the quantification of nucleation rates is difficult. However, figure 2.7 allows to qualitatively understand the nucleation kinetics. Besides these general observations, NPLIN was studied by analyzing it with respect to different factors which are elaborated further in this section. It should be noted that all the subsequent results in this section are expressed as nucleation probability which is equivalent to the cumulative nucleation probability at the end of observation period of 60 minutes.

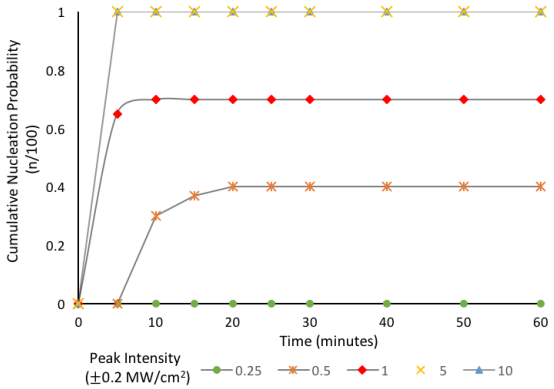

Figure 2.7: (a) Cumulative nucleation probability vs. induction time based on a set of 100 samples. All the samples ($S = 1.055$) were exposed to single pulse of 532 nm light at different peak intensities.

- *Effect of peak intensity*: Peak intensity refers to the energy intensity delivered in a single pulse of laser within a duration of 7 ns. From figure 2.8, a strong dependence of nucleation probability on the peak intensity of laser can be inferred. The results were demonstrated on aqueous KCl solutions with S=1.055 when exposed to a single pulse of 355 nm at varying peak intensities. No nucleation was observed at peak intensity 0.25 MW/cm^2. Generally, the nucleation probability increased with increase in the peak intensity and converged to the probability of 1 at the peak intensity of 5 MW/cm^2. There appears to be a presence of a threshold peak intensity below which no nucleation takes place and a presence of certain saturation peak intensity above which the probability of nucleation is always 1. Due to lack of fine control over the power of the laser, it was difficult to find the exact value of both threshold and saturation peak intensity. However, the significant feature of the result in figure 2.8 is the induction of crystal at the low peak intensity of 0.5 MW/cm^2 which is 10 times smaller than earlier reported threshold intensity of 6 MW/cm^2 for KCl. In contrast 100% nucleation is observed above 5 MW/cm^2 in this work. On further exploration, one of the possible reasons understood for this observation was the difference in the level of impurities in both the systems which has been discussed in detail further in this section.
- *Effect of Wavelength*: The nature of NPLIN was also analyzed by studying the dependence of nucleation probability on the wavelength of the incident beam. The plot in figure 2.9 depicts the observed nucleation probability for solutions with S=1.055 on exposing them to a pulse of different wavelengths of 355, 532 and 1064 nm at different peak intensities. The nucleation probability at 1064 nm is relatively less for low peak intensity of 0.5 and 1 MW/cm^2 as compared to 355 and 532 nm. This can be accounted to the slight absorption of water at 1064 nm which can result in local increase of temperature and consequent decrease in supersaturation. Overall for the three experimental wavelengths, different factors such as fluctuations in room temperature, lack of fine control on laser power especially at low power range, and energy loss due to curvature effects of the vial can also contribute to the differences observed in the nucleation probabilities.
  Besides the trend of nucleation probability with respect to peak intensity remained consistent irrespective of the wavelength. This implies that the nucleation probability was found to increase with increase in peak intensity for each wavelength and the presence of a saturation peak intensity could also be recognized from the 100% probability of nucleating at peak intensities above

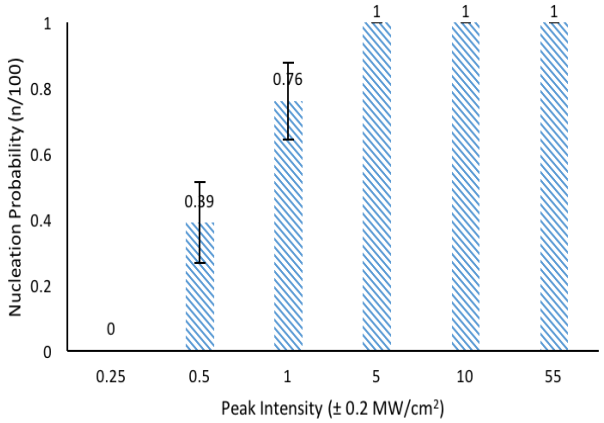

Figure 2.8: Dependence of nucleation probability of NPLIN on peak intensity of 355 nm laser. The nucleation probability is based on a set of 100 samples for S=1.055 and the error bars represent the standard deviation of three experimental trails.

5 MW/cm^2. However, a strong and distinct dependence of wavelength on NPLIN for KCl crystal could not be concluded with the current experimental results.

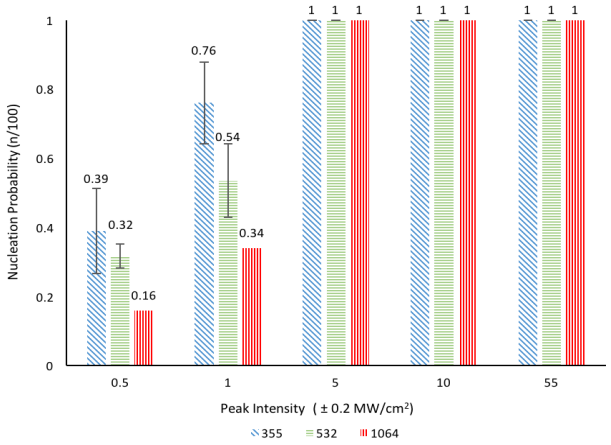

Figure 2.9: Dependence of nucleation probability of NPLIN on different wavelengths namely 355, 532 and 1064 nm. The nucleation probability is based on a set of 100 samples for S=1.055.

- *Effect of Supersaturation*: Supersaturation is the driving force of nucleation which implies that higher the supersaturation, higher is the tendency of the solution to nucleate. The results depicted in the figure 2.10 agree with the aforementioned statement. The results have been demonstrated with a pulse of 532 nm beam for varying peak intensities on both of the supersaturated solutions. A noteworthy inference is that a shift towards both a higher nucleation threshold peak intensity and a saturation peak intensity is observed with a decrease in supersaturation. The change of nucleation threshold with supersaturation is in contradiction with the previously reported supersaturation independent peak intensity threshold in the literature [20].

- *Effect of Impurities*: Although the solutions originally were prepared in accordance with the laboratory standards and utilizing high purity reagents, but it is generally difficult to eliminate the system from all the extrinsic and intrinsic impurities. Extrinsic impurities refer to the impurities which are transferred from the surroundings like dust, whereas the intrinsic impurities refer to the chemical impurities which are associated with the components of the solution. With the intention of studying the effect of these unavoidable impurities, a set of 10 prepared solutions of S = 1.055 were heated and passed through a 0.45 µm sized cellulose acetate membrane filter. The filtered solutions were also found to be stable against spontaneous nucleation for 1-2 weeks.

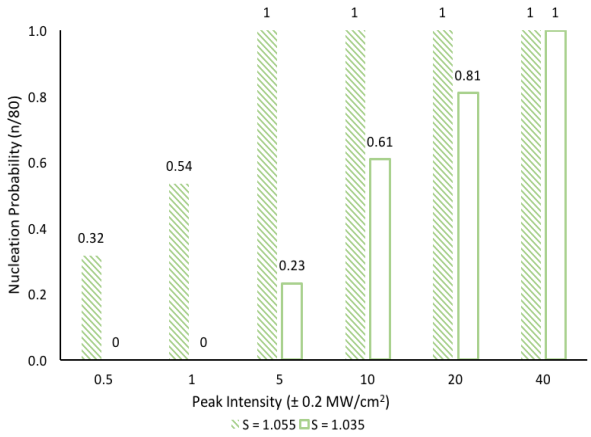

Figure 2.10: Dependence of nucleation probability of NPLIN on supersaturation of S= 1.035 and 1.055. The nucleation probability is based on a set of 80 samples for the wavelength of 532 nm.

Each sample in the set of 10 samples, for both filtered and non-filtered solutions, was exposed to a pulse of 532 nm following the similar experimental procedure as mentioned in section 2.1.3. The effect of impurities on nucleation tendency from laser is evident in figure 2.11. A decrease in nucleation probability is observed with the decrease in the level of impurities in the system. Besides a shift in the nucleation threshold peak intensity and saturation peak intensity is also prominent. It can be argued that the impurities can provide an external surface and promote heterogeneous nucleation. If this was to be true, the unfiltered solutions would have been unstable against spontaneous nucleation. But the unfiltered solutions were stable for a period of 1-2 weeks (equivalent to the filtered solutions), implying that impurities play an important role in enhancing NPLIN.

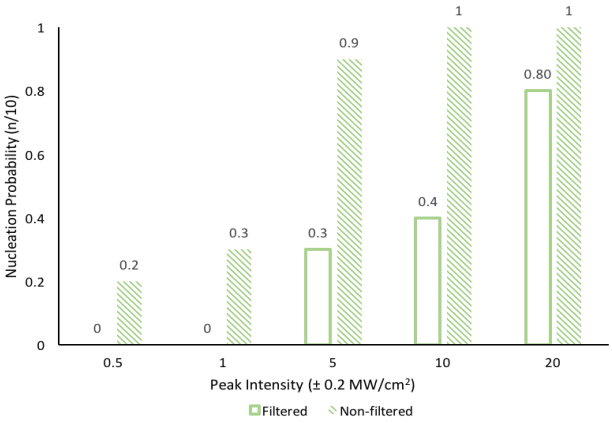

Figure 2.11: Comparison of nucleation probability of NPLIN in unfiltered and filtered KCl solutions of S = 1.055. The nucleation probability is based on a set of 10 samples for the wavelength of 532 nm.

- *Effect of Mixing*: Mixing was introduced in the system by means of a magnetic stirrer and a stirring plate in a batch of 10 solutions for both the supersaturations (S = 1.035 and 1.055). It was observed that spontaneous nucleation was observed on stirring the higher supersaturated solution (S = 1.055), while the lower supersaturation solution was stable under stirred conditions (figure 2.12a). Different literatures highlight the effect of mixing on reducing the MSZW [34, 35]. This can explain the triggering of spontaneous nucleation in higher supersaturation under stirred conditions as stirring can shrink MSZW and push the solution to the labile region of the solubility diagram.
  The effect of stirring on NPLIN was thus studied using the solutions of lower supersaturation (S

= 1.035) to avoid spontaneous nucleation. The stirred solutions were exposed to a pulse of laser at 532 nm and at a fixed peak peak intensity of 5 MW/cm^2. It can be deduced from the figure 2.12b that nucleation probability increases to 80% with stirring in the system as compared to the 10% nucleation probability of the unstirred laser exposed samples. As stirring increases the mass transfer and collision probabilities of solutes, this can exaggerate the nucleation probabilities of NPLIN when the laser passes through the system.

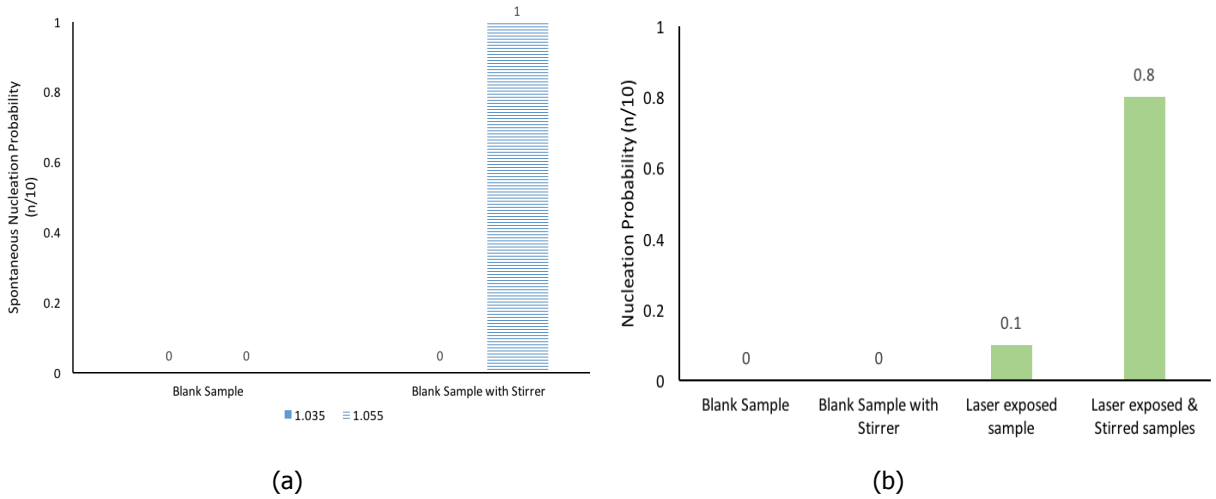

(a) (b)

Figure 2.12: (a) Effect of mixing on the spontaneous nucleation of different supersaturations (S=1.035 & 1.055). (b) Effect of mixing on nucleation probability of solution of lower supersaturation (S=1.035) at a peak intensity of 5 MW/cm^2 and wavelength of 532 nm. Both the results are based on 10 samples of the respective supersaturations.

3

Laser Induced Acoustic Wave

During a curious experiment, a decaying & short-lived pressure wave was detected in the solution immediately after the laser exposure. The very existence of the pressure wave was an unexpected observation as the results from UV-VIS spectroscopy suggested that the system was transparent to the incident beam. On further theoretical and experimental exploration, it was learned that different photo-mechanical and photo-thermal effects can induce an acoustic wave in a transparent solution. This chapter includes a brief introduction about the different mechanisms behind the laser induced acoustic wave, followed by the details of the the experimental procedure and its corresponding results. The experiments were executed with an objective of understanding the nature of the induced acoustic wave and to determine its contribution of KCl.

3.1. Introduction

Due to the capability of pulsed laser to pack energy in a millionth or billionth of a second, high peak intensities and consequently high electric field strengths can be realized. On laser-matter interaction, these high values of electric field strength tend to change the properties of the material and induce non-linear effects in the matter. The generation of the acoustic wave is one such aftereffect which can follow different non-linear mechanisms such as dielectric breakdown, electrostriction, thermo-elastic effect and radiation pressure [36]. The following points concisely describe the different physical phenomena involved in these mechanisms.

- *Dielectric Breakdown*: A dielectric medium becomes conductive above a certain electric strength. The formation of the plasma due to the breakdown of the system leads to induction of a shock wave. This phenomenon becomes prominent at very high peak intensities of laser ($\sim$10 GW/cm^2) [37]. As the experiments in this work are performed in a range of 5 MW/cm^2 to 80 MW/cm^2, thus the high peak intensity threshold required for this mechanism makes its occurrence improbable in our experiments.
- *Electrostriction*: An electromagnetic (EM) wave tends to polarize a dielectric material by inducing dipoles in the material. The strong and non-uniform electric field of the laser changes the mass distribution of the material because the induced dipoles tend to move towards the region of higher electric field strength. These fluctuations in the mass distribution (or density) leads to generation of an acoustic wave in the material [38] (figure 3.1). As electrostriction is an electro-elastic effect, it depends on the incident electric field strength of the EM wave, degree of polarization and the speed of sound in the material. When the EM wave travels through the material, it is difficult for most of the polarization mechanisms to follow the high frequency of the oscillating electric field of the wave which leads to a drop in the degree of polarizability of the system. Thus, electrostriction

becomes dominant only at relatively higher electric field strength for which high peak intensity of laser (>1 GW/cm^2) is required [39]. An elementary estimation calculation given in the appendix A also shows that the magnitude of the pressure associated with the electrostrictive acoustic wave is insignificant in the range of peak intensity of this work and thus can be neglected.

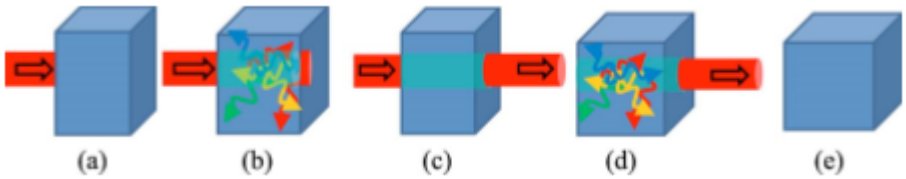

Figure 3.1: Sequential representation of onset of acoustic waves through electrostriction. After the laser beam enters the dielectric transparent medium, it contracts the medium due to the electrostrictive force, sending out acoustic waves as in (b). The contraction remains steady in the system during the pulse width of the beam as in (c). Finally, the material is released from compression stage as the laser leaves the system, releasing acoustic waves as in (d).

- *Thermo-elastic effect*: On laser irradiation, weak linear and non-linear absorption of the medium can produce heat and consequent expansion of the region. In case of pulsed excitation of the medium, the laser pulse is very short which leads to an exceedingly fast thermal expansion and compression. This acoustic wave is detected by the transducer [39]. Any absorption due to the presence of trace amount of dissolved gases and impurities can also contribute to this thermo-elastic effect [40]. This mechanism forms the working principle of the laser photo-acoustic spectroscopy (LPAS) which is used to measure weak linear and non-linear absorption of a system using highly sensitive acoustic detection devices. LPAS technique can measure absorption coefficients as low as 10^{-9} cm^{-1} and detect the presence of trace components with concentration as low as parts per million [41, 42]. The order of magnitude of this effect has been estimated in appendix A.

- *Radiation Pressure*: It is well-understood that EM waves exhibit a dual nature of both a wave and a particle. Owing to the particle nature of EM radiations, light is known to have a momentum associated with it. The existence of this momentum becomes prominent in the 'Radiation Pressure' phenomenon, where the light beam, on travelling through a material medium transfers its momentum to the material media, generating a mechanical pressure in this process. The concept of the radiation pressure when extended to a transparent material medium is developed on the basis of change in velocity of light with change in refractive index (n) of the medium. When the EM radiation passes from air to medium of relatively higher refractive index, the net change in momentum is negative and the consequent pressure involved with this momentum change is a pushing pressure which is also believed to set the fluid into motion [43] (figure 3.2). This interplay of the momentum with matter and the consequent radiation pressure plays an important role in solar sails, optical tweezers, laser-rocket propulsion, etc. Appendix A includes the pressure estimation for this mechanism.

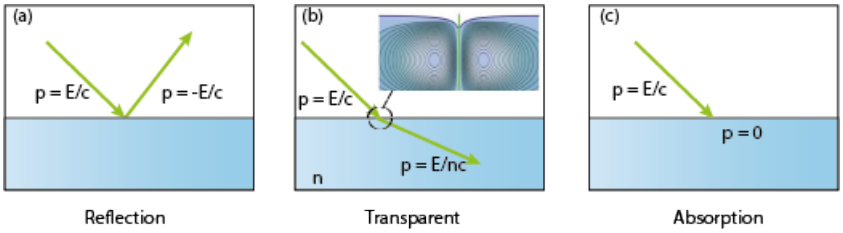

Figure 3.2: The figure represents the momentum change for three different cases of reflection, transparency and absorption where p,E,c and n stands for momentum of light, energy carried by the photons of light, speed of light in air and refractive index of the transparent medium, respectively. The image in (b) represents that the light can induce motion in a transparent dielectric medium. Adapted from [43].

3.2. Materials & Methods

Sigma Aldrich's Methanol (for HPLC, 99%), Sigma Aldrich's Ethanol (for Analytical Grade, 99%), demineralized (DM) water from an in-house dispenser (Elga PURELAB Ultra, 3.7 MΩ.cm) and Radiometer analytical's 0.1 M KCl conductivity standard were the different solvents used during different phases of the experiments. The optical set-up for the generation of laser pulses was similar to the schematics in the previous chapter in figure 2.3. The only addition to the optical set-up of figure 2.3a was a piezoelectric pressure sensor (KISTLER type 601H, range: 0 bar to 1000 bar, sensitivity: $-16\,\mathrm{pC\,bar^{-1}}$) which was submerged in the sample solution for dynamic pressure measurements. The electrostatic charge signal generated by the pressure transducer was further converted to a proportional voltage signal by using a charge amplifier (KISTLER type 5011B, range: 10 pC to 10^5 pC, sensitivity: $0.01\,\mathrm{pC\,bar^{-1}}$ to $10^3\,\mathrm{pC\,bar^{-1}}$). All the signals were analyzed on an oscilloscope procured from Agilent Technologies (DSO-X 3054A).

The solutions were exposed to a single pulse of laser at different peak intensities and wavelengths

(a) (b)

Figure 3.3: Image of (a) the piezoelectric transducer and; (b) the charge amplifier used for pressure measurements of the induced acoustic wave.

at the room temperature (24±1 °C). The corresponding pressure signal from the immersed transducer was recorded in the oscilloscope.

3.3. Results

3.3.1. Characterizing the pressure signal

The insertion of transducer in the supersaturated KCl solution can promote heterogeneous nucleation. Consequently, the formed solid particles can scatter the acoustic wave and alter the transducer's pressure measurements. So to avoid nucleation while pressure measurements, an undersaturated solution of KCl (6.89 mg of KCl / mg of water) was utilized. A volume of 6 ml of the solution was transferred to a borosilicate glass vial. The transducer was inserted into the vial while maintaining a distance of 2.6 cm from the center of the laser beam. The solution was then exposed to a beam of laser of wavelength 532 nm at a peak intensity of $44\,\mathrm{MW/cm^2}$.

Figure 3.4a exemplifies the form of the pressure wave measured by the transducer. A transient pressure disturbance of ms duration was detected in the system on exposing the solution to a 7 ns laser pulse. The pressure signal was always measured to be in the range of mbar. The relaxation time of the wave is approximated as the time taken by the signal to drop to the noise level of the transducer. For the signal in figure 3.4a, the relaxation time approximates to 3.5 ms. The subsequent results are reported in terms of maximum amplitude of the pressure signal (P) which is calculated using the maximum peak to peak distance of a pressure waveform as shown in figure 3.4a. It was also observed that on frequently exposing the solution to laser pulses, the maximum pressure amplitude of the wave was found to decrease with every pulse (figure 3.4b). The observations in figure 3.4 are consistent with the literature reported observations for photo-acoustics of thermo-elastic effects of laser [44]. The trend in figure 3.4b strongly suggests that the thermo-elastic effects of laser play an important role in inducing the acoustic wave.

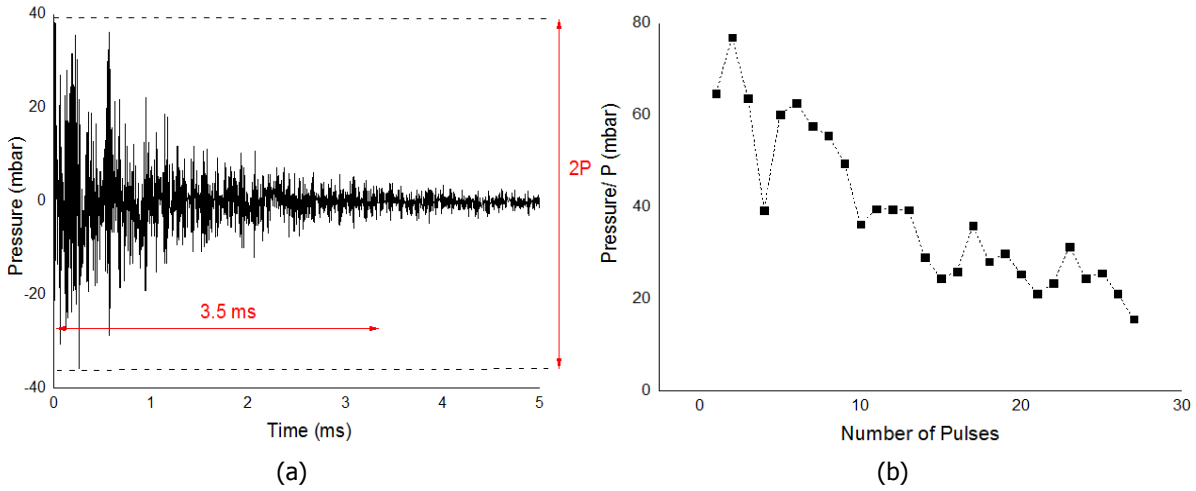

Figure 3.4: (a) An example of laser induced acoustic wave showing the relaxation time of the waveform and the maximum pressure amplitude (P) of the waveform; (b) Decreasing maximum pressure amplitude of the acoustic wave on exposing the solution to pulses with a frequency of 1 Hz. KCl (0.1 M) solution was exposed to the beam of 532 nm at a peak intensity of 44 MW/cm^2.

The time lag between the laser pulse and the pressure signal was found by simultaneously analyzing the signals from photo-detector and the transducer. As the photo-detector has a quick rise time of 1 ns, it enables to detect the travelling laser beam. Figure 3.5 represents the time lag between the laser pulse and the onset of the acoustic wave. Assuming that the acoustic wave emerges from the path of the laser, the time lag arises because the acoustic wave has to travel a distance of 2.6 cm to reach the transducer. This assumption allows to compute the speed of the acoustic wave to be around 1383 m/s. This is in close approximation to the speed of sound in KCl solution (1468 m s^{-1}) as mentioned in the literature [45]. Thus, the induced pressure wave can be called as an acoustic wave which exists in the system for a period of 3 ms to 4 ms before attenuating completely.

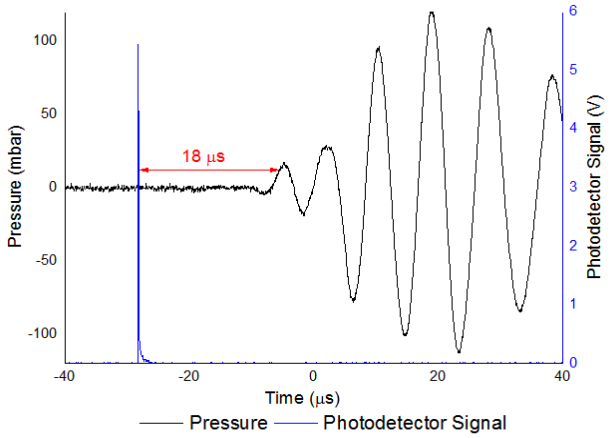

Figure 3.5: Time lag between the laser pulse and the onset of the pressure fluctuations. The aqueous solution of KCl was exposed to single pulse of 532 nm at a peak intensity of 44 MW/cm^2.

3.3.2. Effect of wavelength and peak intensity on the acoustic wave

In order to understand the nature of acoustic wave, the undersaturated solution of KCl was exposed to a pulse of laser at different wavelengths and peak intensities. The acoustic wave prevailed in the system irrespective of the incident wavelength and the maximum amplitude of the pressure of the wave increased with increase of incident peak intensity (figure 3.6). On that account, the amplitude of

acoustic wave showed a similar dependency on peak intensity as NPLIN. But unlike NPLIN, no saturation peak intensity was observed for the acoustic wave. It was also difficult to point out the presence of a threshold peak intensity for the induced wave as the pressure signals dropped to the noise level of the transducer (±1.5 mV) below the laser's peak intensity of 6 MW/cm^2.

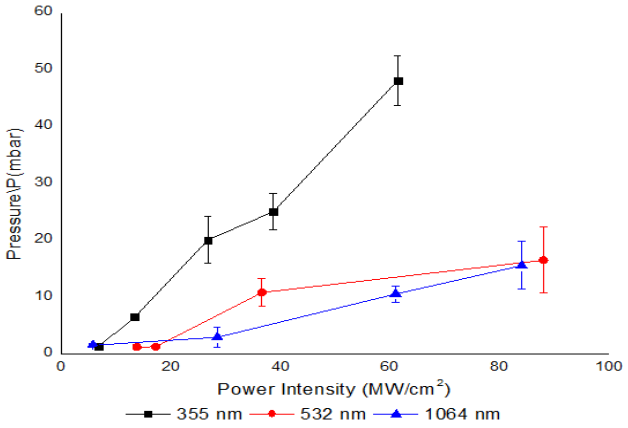

Figure 3.6: Variation of maximum pressure amplitude of laser induced acoustic wave with peak intensity and wavelength. The results are based on the acoustic wave induced from single pulse of laser in 0.1M KCl solution.

The relaxation time of the signal remained the same (∼3 ms) regardless of the incident wavelength and peak intensity. On comparing the maximum amplitudes of the pressure signal for different wavelengths, the amplitudes were found to be higher for 355 nm than 532 and 1064 nm. Based on the theoretical understanding so far, two factors can be accounted for this anomaly. Firstly, it could be due to the differences in the transparency of the borosilicate glass vials at these respective wavelengths. As from the figure 2.3b, the transparency of the borosilicate glass is lower at 355 nm than at 532 and 1064 nm, so more reflection and scattering of laser can be expected at 355 nm which enhances the radiation pressure exerted on the system. Secondly, 355 nm could excite non-linear absorption of the solution and/or the trace impurities present in the KCl solution for thermo-elastic mechanism.
In a different experiment, it was observed that the pressure amplitudes for the laser induced acoustic waves were different for different sources of water. On exposing the tap water to single pulse of 532 nm at a peak intensity of 40 MW/cm^2, the maximum pressure amplitude measured was 76 mbar which dropped to 4 mbar for DM water. This indicates that impurities play a role in the mechanism of laser induced acoustic wave. This observation strengthens the assumption that selective absorption of the impurities in the KCl solution can also lead to the higher pressure signal (figure 3.6). However, further in-depth experimental and theoretical analysis is required to understand the behaviour of the acoustic waves at different wavelengths.

3.3.3. Effect of different solvents on the acoustic wave

The laser induced acoustic wave was also detected in three commonly used solvents namely ethanol, methanol and DM water. The bulk transparency of these solutions at 532 nm has been reported in literature. The solutions were exposed to a single pulse of 532 nm at peak intensity of 80 MW/cm^2. A relatively high peak intensity of 80 MW/cm^2 was chosen to have a high signal to noise ratio. No significant difference was observed in the relaxation times of the acoustic wave for methanol, ethanol and KCl (figure 3.7). But the acoustic wave for DM water showed a relatively shorter life span of 2 ms.
The form of the acoustic wave and the maximum amplitude of the pressure signal varied with different solvents. The graph in figure 3.8 represents the overall trend measured for the pressure associated with the acoustic wave in the respective solutions. Since the solutions were exposed to similar optical conditions, it can be assumed that the magnitude of the radiation pressure remains the same in all the cases. Thus, a major contribution to the pressure variation comes from the mechanism of thermo-elastic effect. As this mechanism involves a thermo-elastic change in the system, it should be

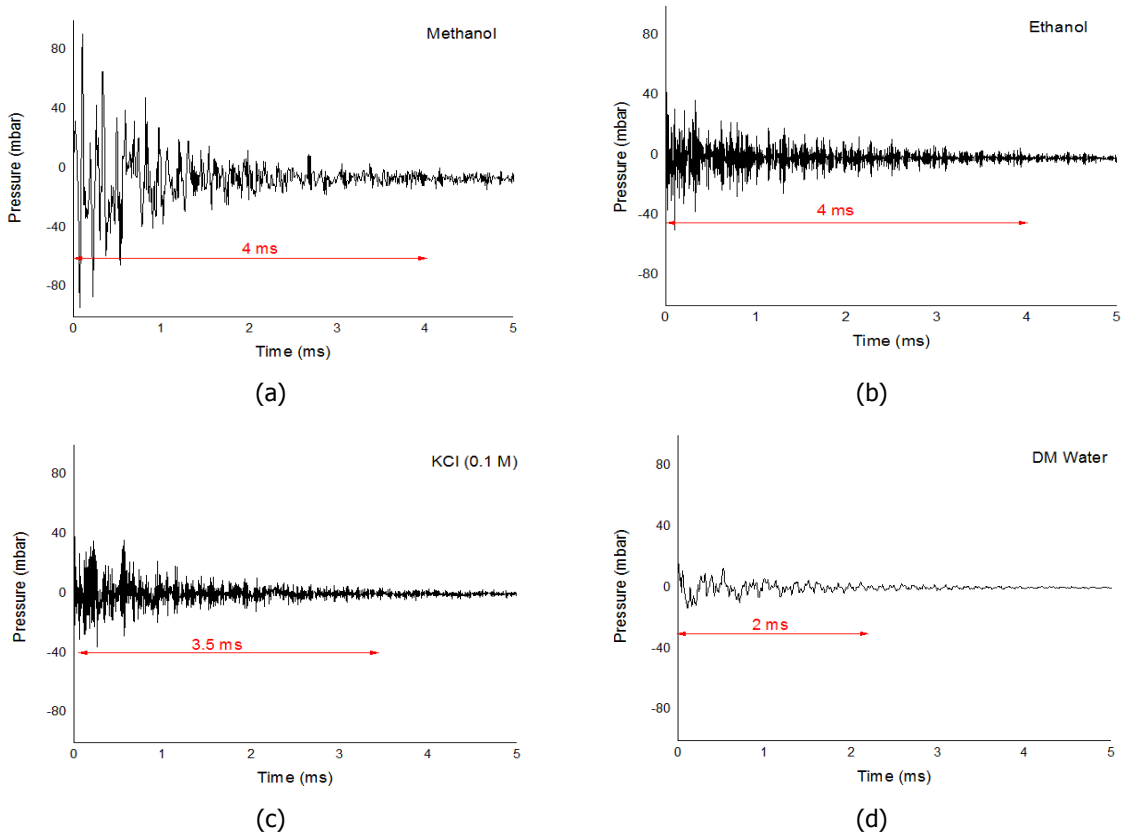

Figure 3.7: Acoustic waveform for (a) Methanol; (b) Ethanol; (c) KCl (0.1 M); (d) DM water. All the solutions were exposed to single pulse of 532 nm laser at 80 MW/cm^2

affected by the thermal and elastic properties of the solutions. In the work by Patel *et al.*, the pressure amplitude for the thermo-elastic acoustic wave induced by a short laser pulse for nearly transparent liquids is defined using the Grüneisen coefficient. This coefficient lumps together the thermal expansion coefficient (β), speed of sound (v), and thermal capacity (C_P) of the solution. The pressure amplitude (P) for thermo-elastic wave is proportional to Grüneisen coefficient.

$$P \propto \frac{\beta\, v^2}{C_P} \tag{3.1}$$

The value of the Grüneisen coefficient has been tabulated in Table 3.1 for the respective solutions by using the literature reported values of β, C_P and v.

Solution	β (10^{-3} K^{-1})	C_P (J g^{-1} K^{-1})	v (m s^{-1})	$\frac{\beta v^2}{C_P}$ (10^{-5} kgm^2/J/s^2)
Methanol	1.05	2.48	1144	48
Ethanol	1.02	1.41	1100	79
KCl (0.1 M)	0.35	1.02	1468	49
DM water	0.2	4.18	1464	7

Table 3.1: Literature reported values for thermal expansion coefficient (β), speed of sound (v), and thermal capacity (C_P) and the corresponding value of Grüneisen coefficient ($\frac{\beta v^2}{C_P}$) for different solvents.

From the computed values in table 3.1, it is evident that the value of the Grüneisen coefficient for DM water is an order of magnitude less as compared to the values for other solvents. This explains the relatively less magnitude of pressure signal measured for DM water. But it is difficult to explain the exact the trend with the values in table 3.1.

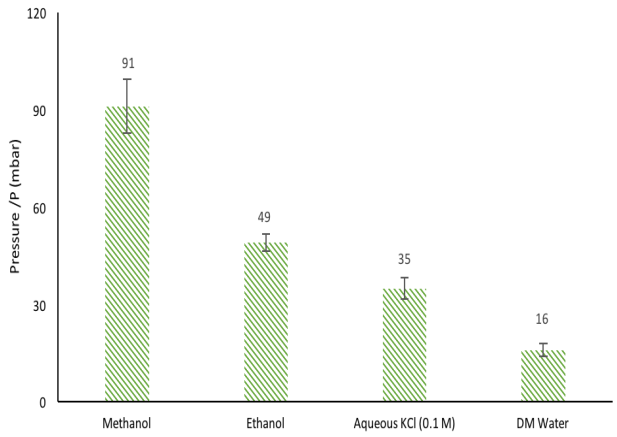

Figure 3.8: Variation of maximum pressure amplitude of laser induced acoustic wave in different solvents. The results are based on acoustic wave induced from single pulse of 532 nmlaser at 80 MW/cm^2.

3.3.4. Effect of different containers on the acoustic wave

The characteristics of the laser induced acoustic wave were investigated by confining ethanol in different containers and exposing it to a single pulse of 532 nm at 80 MW/cm^2. Three different containers were used whose construction material, geometry, and the laser irradiated volume of ethanol are tabulated in the table 3.2.

Experiment Container	Material	Geometry	Exposed volume (mm^3) (approx.)
Vial (8 ml)	Borosilicate glass	Cylindrical	326
OG Cuvette	Optical glass (OG)	Rectangular	196
Beaker (100 ml)	Borosilicate glass	Cylindrical	1138

Table 3.2: Details of the different containers used to study the characteristics of the laser induced acoustic wave.

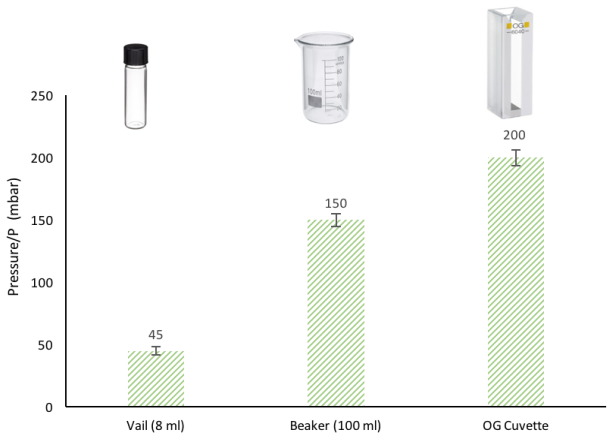

Figure 3.9: Variation of pressure amplitude of laser induced acoustic wave when the solution is confined in containers of different geometries and volumes. The results are based on exposure of ethanol to a single pulse of 532 nm laser at a peak intensity of 80 MW/cm^2.

Figure 3.9 represents the trend of pressure signal observed for the different cases. On comparing the pressure amplitudes measured in the two borosilicate cylindrical vessels, it can be inferred that the amplitude of the wave increases with the increase of volume. This can be explained from the fact that if more volume is exposed to the laser, more excitation from the thermo-elastic effect can take place. However, for the OG cuvette, the volume exposed to the solution is the least but the measured pressure signal is still considerably higher than the experiments executed in the borosilicate

glass containers. This can be attributed to the higher transparency of the optical glass as compared to the borosilicate glass. Moreover, OG cuvette has a rectangular geometry and thus experiences less scattering as compared to the circular curvature of the glass vials. Less scattering of the laser implies that the solution in the OG cuvette is exposed more efficiently. Also, it has been reported that the two parallel faced geometry acts as an ideal example for resonating the acoustic signals [46]. This implies that the higher signals in the cuvette could be due to resonance of the wave owing to the rectangular geometry of the cuvette. The induced acoustic waveform for the three containers are included in the appendix B.

3.3.5. Effect of acoustic wave on NPLIN

Although, further experimental validation is required to confirm the exact mechanisms behind laser induced acoustic wave. Nevertheless, the executed experiments have provided enough evidence regarding the induction of an pressure wave on laser exposure. Since, it is known that mechanical shocks can also induce nucleation through shear, it makes it important to analyze the influence of the induced acoustic wave on NPLIN [13]. For this purpose, a portion of the vial was covered using a masking tape (figure 3.7b). The masking tape prevented the laser from entering the solution by absorbing it. This was confirmed by the power meter measurements as no power was detected after the vial. On exposing the masked vial to laser, a stronger pressure signal was detected in the masked glass vial than the unmasked ones (figure 3.7a). Both the vials were exposed to a pulse of 532 nm and 80 MW/cm^2. Further 100 masked and unmasked vials with supersaturated aqueous KCl solutions of S= 1.035 &

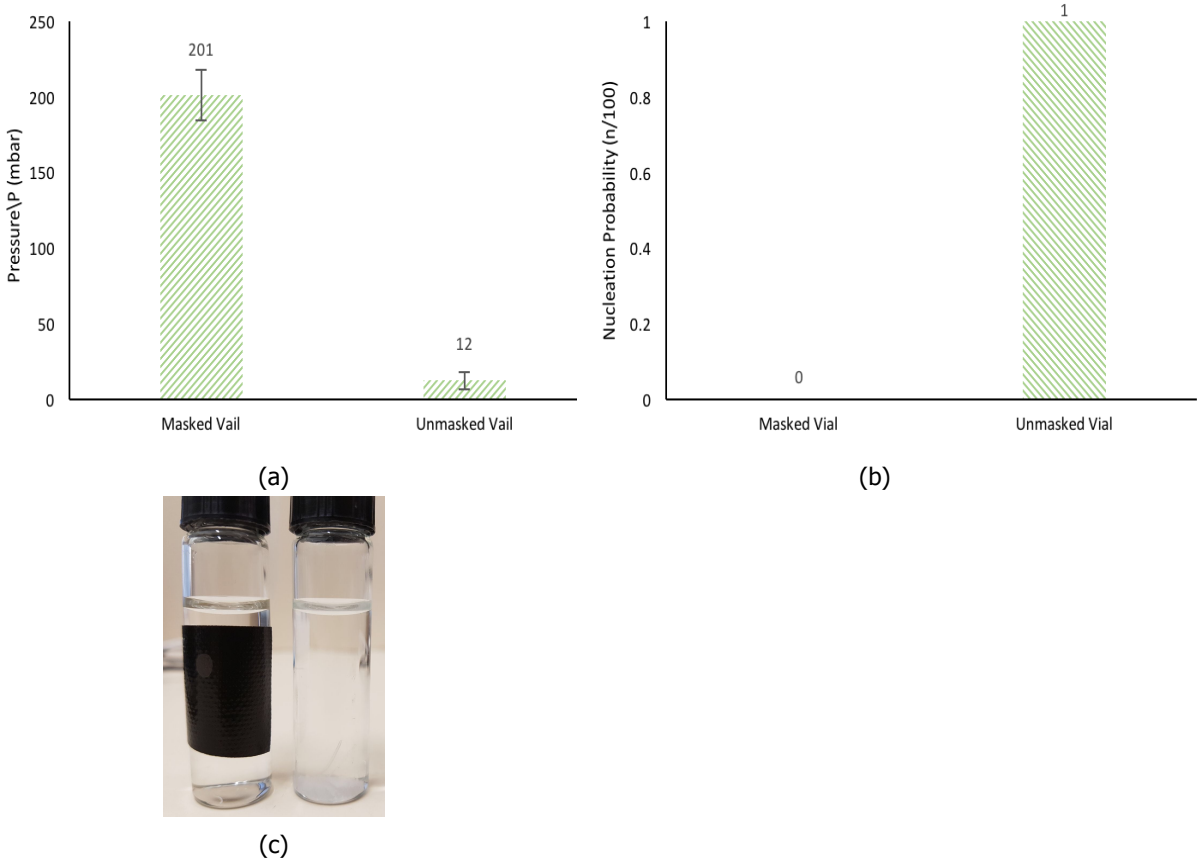

Figure 3.10: (a) Comparison of the measured pressure amplitudes and; (b) nucleation probabilities of the masked and the unmasked vial on laser exposure. (c) Image showing the masked and unmasked vial. The crystals formed on the laser exposure, can be seen settled at the bottom of the unmasked vial. The solutions were exposed to a pulse of 532 nm at a peak intensity of 44 MW/cm^2.

1.055 were exposed to a single pulse of 532 nm laser at a peak intensity of 80 MW/cm^2. However,

no nucleation was observed in the masked vials whereas all the unmasked vials showed immediate formation nuclei on laser exposure. These observations allow to reach a conclusion that an acoustic wave is induced due to laser. The trends from the different analyses suggest that the thermo-elastic effects and radiation pressure contribute significantly in the induction of the acoustic wave. But the corresponding pressure fluctuations from the induced wave are not high enough to induce nucleation in the supersaturated solution.

4

Discussion, Conclusions & Recommendations

In the previous chapters, different factors were analyzed to determine their effect on the efficiency of NPLIN. It is important to interpret these results in accordance to the different proposed hypotheses, so as to develop a mechanistic understanding of NPLIN. This is qualitatively developed in the discussion section of this chapter followed by the conclusions of this work and few recommendations for the future work.

4.1. Discussion

In this work, it is observed that NPLIN is strongly influenced by the peak intensity of laser (figure 2.8). The peak intensity can be directly related to the electric field strength (E) of laser by

$$I = \frac{1}{2}\, c\, \epsilon_0\, E^2 \tag{4.1}$$

where the peak intensity (I) is also dependent on the speed of light in vacuum (c) and vacuum's permittivity (ϵ_0). While the peak intensity has a quadratic dependence on electric field, it is independent of the wavelength of the incident beam. This characteristic is consistent with the observations of this work as NPLIN also showed a weak dependence on wavelength (figure 2.9). In literature, the laser induced nucleation of KCl has been explained using the hypothesis of isotropic electronic polarizability [20]. Although, the mechanism of OKE fails to explain the nucleation of isotropic clusters of KCl but various literatures have reported the dependence of polymorphism on the polarization of the incident beam [18, 22]. Thus, the evidence from the literature is too strong to neglect the hypothesis of OKE. Moreover, the mechanism of OKE is also dependent on the electric field strength of the beam.

Further, it is observed that the presence of impurities in the system can influences the activity of NPLIN. This observation highlights the fact that the mechanism of NPLIN is also affected by light-impurity particle interaction and not just interaction of light and pre-nucleating solute clusters. It can also be argued that the laser can interact with the ansiotropic polarizability of the impurities to induce the phenomenon of polarization switching. However, this hypothesis requires further experimental investigations.

Lastly, Nasrin *et al.* suggested that nucleation could also be induced from the laser induced sound wave [29]. They demonstrate this by using high laser peak intensities of 10 TW/cm^2. It is possible that at such high intensities of focused lasers, different non-linear mechanisms such as multi-photon absorption, dielectric polarization and high radiation pressure can induce a strong compression wave in the solution. However, for the range of low peak intensities of unfocused laser, a weak acoustic wave is induced in the system. Using the calculations in appendix A, it is estimated that unfocused laser

induces an acoustic wave with pressures fluctuating in mbar. It was experimentally demonstrated in this work that acoustic waves cannot alter the nucleation kinetics of NPLIN.

Thus, for unfocused laser radiation of lower peak intensity, the interaction of laser and matter is essential to induce nucleation. Also based on the current experimental results, this laser-matter interaction appears to be a multi-mechanistic process where different non-linear mechanisms can collectively contribute to account for the observed enhancement of the nucleation kinetics.

4.2. Conclusion

In this research, laser induced non-photochemical nucleation phenomenon is studied for aqueous supersaturated solutions of KCl. Different parameters were analyzed to understand the nature of NPLIN using a large sample set of 80-100 samples for each of the parameters. Nucleation efficiency of laser was determined to be largely dependent on the peak intensity of laser with a presence of threshold and saturation peak intensity. Importantly, nucleation was observed at relatively low peak intensities of laser at 0.5 MW/cm^2, which is 10 times lower than the earlier reported threshold peak intensity for KCl. The effect of three different wavelengths of 355, 532 and 1064 nm was also investigated in this research which lead to a conclusion that the nucleation efficiency of laser showed a weak dependence on the incident wavelength of the beam.

Nucleation efficiency for two different supersaturations with S = 1.035 & 1.055 were analyzed. The experiments yielded the expected result of increase in nucleation efficiency on increasing the supersaturation. It was also noted that filtering of the samples prior to studying the laser induced nucleation resulted in the lowering of nucleation probabilities, highlighting the role of sub-micron impurities in enhancing NPLIN.

Further, the laser induced acoustic wave was detected by immersing the piezo-electric transducer in the solution. Different experiments were executed to understand the nature and origin of the acoustic wave. It was inferred that the acoustic wave was induced in the solution due to the non-linear laser matter interaction. Additionally, the experiments also aided in concluding that the laser induced acoustic wave didn't induce nucleation for the experimental peak intensity range. Overall, the results show that several mechanisms can contribute to the process of NPLIN.

To summarize, NPLIN certainly enhances the nucleation kinetics and provides an opportunity for inducing nucleation without utilizing any chemical additives. However, non-photochemical laser induced nucleation as a process is still in its infancy and requires further work to fully explore the potential of this technique.

4.3. Recommendations

- *Fine control over peak intensity*: During the course of experiments, it was difficult to establish a precise control over the power output of the laser pulse. It is recommended to develop a better optical set-up utilizing the combination of wave-plates and polarizers. A fine control over power will allow to precisely study the dependency of peak intensity on the efficiency of NPLIN.
- *Doping of the supersaturated solutions*: Thorough investigations need to be implemented to understand the effect of impurities on the nucleation efficiency of laser. The supersaturated solutions can be intentionally doped to understand the influence of different chemical impurities. Also, the experiments can be recorded with a high frame rate camera to observe any formation of micro-bubbles on laser exposure.
- *Improving statistical quality*: In this work, 100 samples were utilized to obtain a single data point. The present experimental scheme is slow and consumes large amount of chemicals to build the statistical quality of the work. Instead of using bulk solution, this can be achieved by designing a microfluidic set-up where large number of samples can be generated and the nature of NPLIN can be studied more efficiently.
- *Visual recording using sophisticated imaging system*: While experimenting in bulk solution, the region of interest (ROI) becomes too vast and it becomes difficult to exactly locate the formation

of nuclei. Thus, experimenting in micro scale reduces the ROI spatially and makes it relatively easier to visually record the event of nucleation on laser exposure.

A

Order of Magnitude Estimation for Laser Induced Acoustic Wave

Elementary calculations were carried out to estimate the order of magnitude for the induced pressure due to different non-linear mechanisms.

- *Electrostriction*: The electrostriction mechanism is based on the non-uniformity of the electric field. For the case of laser, non-uniformity exists for both temporal and spatial dimensions due to the Gaussian distribution of laser beam's intensity. Thus, the expression for non-uniform squared electric field of the laser beam varying radially with r and time, t, is defined as follows,

$$E^2(r,t) = E^2(r)T(t), \tag{A.1}$$

with

$$E^2(r) = \frac{2\,I}{\pi\,\epsilon_0\,n\,c}\,exp[-\frac{2\,r^2}{w_0^2}] \tag{A.2}$$

where I is the incident peak intensity, ϵ_0 is the vacuum's permittivity, c is the speed of light in air, n is the refractive index of medium and w_0 is the radius of the laser beam [47]. For simplicity, the temporal Gaussian evolution of laser wasn't accounted. Instead, it was assumed that the laser beam evolves as a step-function. Thus, for a laser pulse originating at $t = 0$ with a pulse width of t_0, the temporal evolution, $T(t)$, is defined as

$$T(t) = \begin{cases} 0 & \text{if } t < 0 \text{ or } t > t_0 \\ 1 & \text{if } 0 \le t \le t_0 \end{cases} \tag{A.3}$$

This implies that during the entire pulse width of the laser beam, the material experiences the maximum electrostrictive pressure. The electrostrictive pressure, $P_{es}(r)$, due to the presence of beam is expressed as

$$P_{es}(r) = \frac{1}{6}\,\epsilon_0\,E^2(r)\,(n^2-1)\,(n^2+1), \tag{A.4}$$

which on substitution of equation A.2 yields

$$P_{es}(r) = \frac{(n^2-1)\,(n^2+1)\,I}{3\,\pi\,n\,c}\,exp[-\frac{2\,r^2}{w_0^2}]. \tag{A.5}$$

It should be noted that equation A.5 provides the value for electrostrictive pressure exerted by the source. It doesn't represent the bulk pressure developed in the fluid as that would require a detailed analysis using Navier–Stokes equations. Nevertheless, the results from the equation

A.5 provide an ideal case and consequently the best case scenario for the order of magnitude estimation. The results in figure A.1 show that in an ideal case, the electrostrictive pressure would be of order $\sim 10^{-7}$ bar. However, in reality, the electrostrictive pressure would be further lower than the results of figure A.1 due to the fluid's inertia. Thus, electrostriction is not a dominant phenomena for inducing acoustic wave in our experiments.

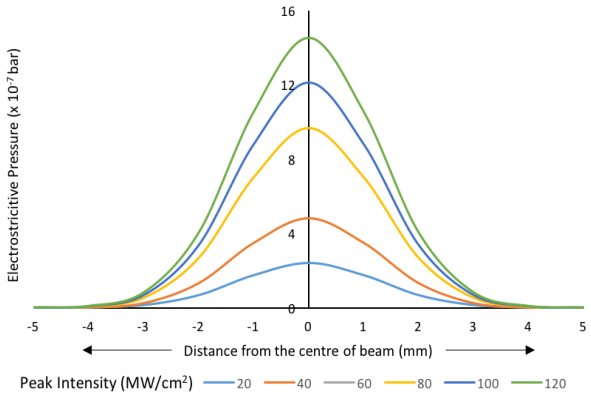

Figure A.1: Estimation of the electrostrictive pressure experienced in the radial path of beam for different peak intensities.

- *Thermal effect*: In case of very small absorption coefficients, the penetration of light in the medium is much larger than the diameter of the beam itself. For this reason, the source of the acoustic wave can be assumed to be cylindrical. For a short pulse duration, the amplitude of the pressure (P) for a cylindrical acoustic wave is defined by the following empirical equation,

$$|P| = \frac{E\,\alpha\,\beta\,v^2}{C_P\,R_S^{\frac{3}{2}}\,r^{\frac{1}{2}}} \tag{A.6}$$

where E is the energy intensity of the incident beam, α is the absorption coefficient of the liquid, β is the thermal expansion coefficient, v is the speed of the acoustic wave in the liquid, C_P is the liquid's specific heat, R_S is the radius of the acoustic source and r is the distance between the source and the detector. Assuming the radius of the acoustic source to be equivalent to the radius of the incident beam i.e. 2.5 mm and further substituting the value of thermal parameters (table 3.1) for water in equation A.6, the pressure amplitudes for different peak intensities are plotted in figure A.2. The graph represents the pressure amplitude for pure water medium in the visible region using the absorption coefficient of $10^{-4}\,\mathrm{cm}^{-1}$ [48]. As the computed amplitude of the pressure is in range with the experimental observations of this work, thermo-elastic effect can be one of the prominent phenomenon responsible for photo-acoustics.

- *Radiation Pressure*: The linear momentum (p) arising from the translational motion of the elementary particles of the EM waves (photons) is expressed as

$$p = \frac{\text{Energy carried by the wave } (E)}{\text{speed of light in vacuum } (c)} \tag{A.7}$$

Further, radiation pressure (P_{rad}) is defined as the rate of change of momentum of the EM wave per unit area and is expressed using the peak intensity of light (I) and speed of light in vacuum (c),

$$P_{rad} = \frac{\frac{dp}{dt}}{Area} = \frac{I}{c} \tag{A.8}$$

The radiation pressure for three different cases of absorption, reflection and in transparent

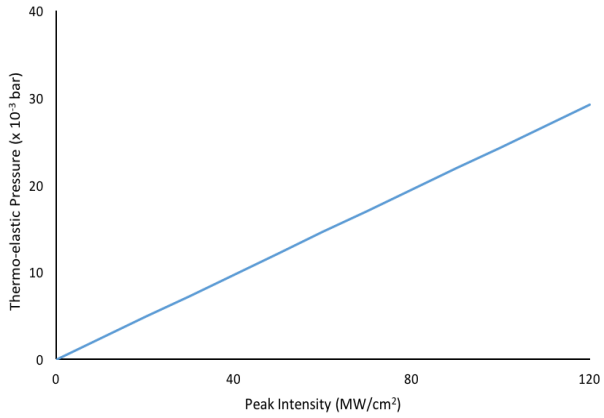

Figure A.2: Amplitude of the pressure due to thermo-elastic effects induced in pure water by laser of wavelength in the visible region.

medium (of refractive index, n) is defined as [43]

$$|P_{rad}| = \begin{cases} \frac{I}{c} & \text{Absorption} \\ \frac{2\,I}{c} & \text{Reflection} \\ \frac{I}{c}\left(\frac{1-n}{n}\right) & \text{Transparent} \end{cases} \tag{A.9}$$

This estimation also doesn't take into account the dampening of the wave due to the fluid's

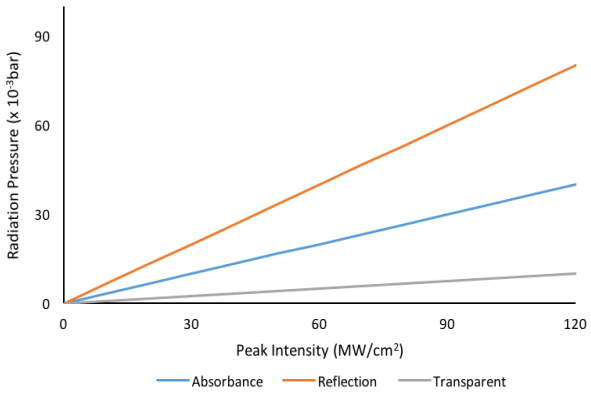

Figure A.3: Maximum amplitude of the radiation pressure of a beam for three different cases of absorption, reflection and the pressure exerted in a transparent medium with refractive index equivalent to water.

inertia, but the order of magnitude of the estimated radiation pressure is in the range of the experimental observations. Thus, this mechanism can also be one of the contributors to the induced acoustic wave.

B

Induced Acoustic Waveform for Different Containers

The graphs in figure B.1 represent the wave form and the corresponding life-span for the acoustic wave induced in ethanol enclosed in different containers.

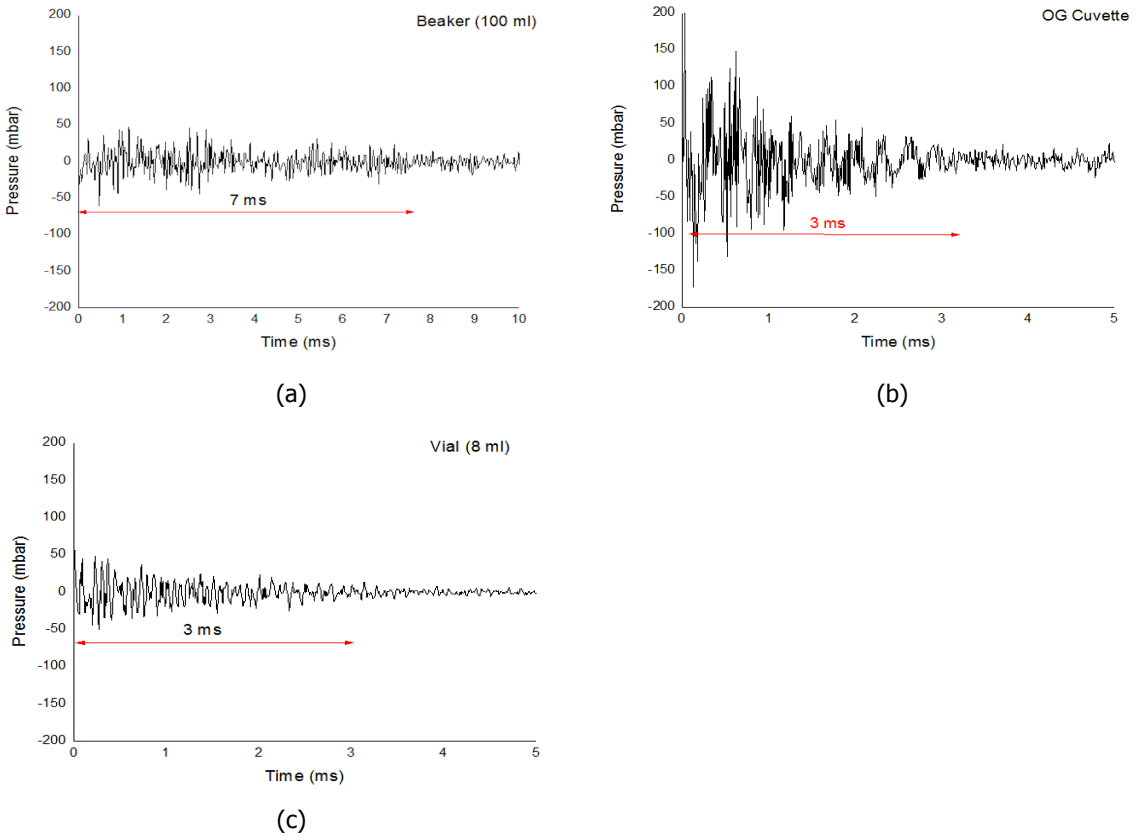

Figure B.1: Acoustic waveform induced in ethanol enclosed in (a) borosilicate beaker (100 ml); (b) OG Cuvette; and (c) borosilicate vial on exposing it to a pulse of 532 nm and peak intensity of 80 MW/cm^2.

Bibliography

[1] M. L. de Castro and F. Priego-Capote, "Ultrasound-assisted crystallization (sonocrystallization)", *Ultrasonics Sonochemistry*, vol. 14, no. 6, pp. 717–724, 2007, ISSN: 1350-4177. DOI: http://dx.doi.org/10.1016/j.ultsonch.2006.12.004. [Online]. Available: http://www.sciencedirect.com/science/article/pii/S1350417706001684.

[2] N. Radacsi, J. H. ter Horst, and G. D. Stefanidis, "Microwave-assisted evaporative crystallization of niflumic acid for particle size reduction", *Crystal Growth & Design*, vol. 13, no. 10, pp. 4186–4189, 2013. DOI: 10.1021/cg4010906. eprint: http://dx.doi.org/10.1021/cg4010906. [Online]. Available: http://dx.doi.org/10.1021/cg4010906.

[3] R. Kacker, P. M. Salvador, G. S. J. Sturm, G. D. Stefanidis, R. Lakerveld, Z. K. Nagy, and H. J. M. Kramer, "Microwave assisted direct nucleation control for batch crystallization: Crystal size control with reduced batch time", *Crystal Growth & Design*, vol. 16, no. 1, pp. 440–446, 2016. DOI: 10.1021/acs.cgd.5b01444. eprint: http://dx.doi.org/10.1021/acs.cgd.5b01444. [Online]. Available: http://dx.doi.org/10.1021/acs.cgd.5b01444.

[4] D. Hou and H.-C. Chang, "Ac field enhanced protein crystallization", *Applied Physics Letters*, vol. 92, no. 22, p. 223 902, 2008. DOI: 10.1063/1.2938887. eprint: http://dx.doi.org/10.1063/1.2938887. [Online]. Available: http://dx.doi.org/10.1063/1.2938887.

[5] Z. Hammadi and S. Veesler, "New approaches on crystallization under electric fields", *Progress in Biophysics and Molecular Biology*, vol. 101, no. 1, pp. 38–44, 2009, Novel Approaches to Protein Crystallization and Crystal Quality Enhancement, ISSN: 0079-6107. DOI: http://dx.doi.org/10.1016/j.pbiomolbio.2009.12.005. [Online]. Available: http://www.sciencedirect.com/science/article/pii/S0079610709000856.

[6] H. Koizumi, K. Fujiwara, and S. Uda, "Control of nucleation rate for tetragonal hen-egg white lysozyme crystals by application of an electric field with variable frequencies", *Crystal Growth & Design*, vol. 9, no. 5, pp. 2420–2424, 2009. DOI: 10.1021/cg801315p. eprint: http://dx.doi.org/10.1021/cg801315p. [Online]. Available: http://dx.doi.org/10.1021/cg801315p.

[7] C. Sudha, R. Sivanarendiran, and K. Srinivasan, "Influence of magnetic field on the nucleation rate control of mono paracetamol", *Crystal Research and Technology*, vol. 50, no. 3, pp. 230–235, 2015, ISSN: 1521-4079. DOI: 10.1002/crat.201400432. [Online]. Available: http://dx.doi.org/10.1002/crat.201400432.

[8] B. A. Garetz, J. E. Aber, N. L. Goddard, R. G. Young, and A. S. Myerson, "Nonphotochemical, polarization-dependent, laser-induced nucleation in supersaturated aqueous urea solutions", *Phys. Rev. Lett.*, vol. 77, pp. 3475–3476, 16 Oct. 1996. DOI: 10.1103/PhysRevLett.77.3475. [Online]. Available: https://link.aps.org/doi/10.1103/PhysRevLett.77.3475.

[9] J. Zaccaro, J. Matic, A. S. Myerson, and B. A. Garetz, "Nonphotochemical, laser-induced nucleation of supersaturated aqueous glycine produces unexpected γ-polymorph", *Crystal Growth & Design*, vol. 1, no. 1, pp. 5–8, 2001. DOI: 10.1021/cg0055171. eprint: http://dx.doi.org/10.1021/cg0055171. [Online]. Available: http://dx.doi.org/10.1021/cg0055171.

[10] A. K. E.-Z. El-Yafi and H. El-Zein, "Technical crystallization for application in pharmaceutical material engineering: Review article", *Asian Journal of Pharmaceutical Sciences*, vol. 10, no. 4, pp. 283–291, 2015, ISSN: 1818-0876. DOI: http://dx.doi.org/10.1016/j.ajps.2015.03.003. [Online]. Available: http://www.sciencedirect.com/science/article/pii/S1818087615000264.

[11] N. Kubota, "A new interpretation of metastable zone widths measured for unseeded solutions", *Journal of Crystal Growth*, vol. 310, no. 3, pp. 629–634, 2008, ISSN: 0022-0248. DOI: http://dx.doi.org/10.1016/j.jcrysgro.2007.11.123. [Online]. Available: http://www.sciencedirect.com/science/article/pii/S0022024807011153.

[12] S. S. Kadam, S. A. Kulkarni, R. C. Ribera, A. I. Stankiewicz, J. H. ter Horst, and H. J. Kramer, "A new view on the metastable zone width during cooling crystallization", *Chemical Engineering Science*, vol. 72, pp. 10–19, 2012, ISSN: 0009-2509. DOI: http://dx.doi.org/10.1016/j.ces.2012.01.002. [Online]. Available: http://www.sciencedirect.com/science/article/pii/S0009250912000048.

[13] J. Mullin, "5 - nucleation", in *Crystallization (Fourth Edition)*, J. Mullin, Ed., Fourth Edition, Oxford: Butterworth-Heinemann, 2001, pp. 181–215, ISBN: 978-0-7506-4833-2. DOI: https://doi.org/10.1016/B978-075064833-2/50007-3. [Online]. Available: http://www.sciencedirect.com/science/article/pii/B9780750648332500073.

[14] D. Erdemir, A. Y. Lee, and A. S. Myerson, "Nucleation of crystals from solution: Classical and two-step models", *Accounts of Chemical Research*, vol. 42, no. 5, pp. 621–629, 2009, PMID: 19402623. DOI: 10.1021/ar800217x. eprint: http://dx.doi.org/10.1021/ar800217x. [Online]. Available: http://dx.doi.org/10.1021/ar800217x.

[15] S. Karthika, T. K. Radhakrishnan, and P. Kalaichelvi, "A review of classical and nonclassical nucleation theories", *Crystal Growth & Design*, vol. 16, no. 11, pp. 6663–6681, 2016. DOI: 10.1021/acs.cgd.6b00794. eprint: http://dx.doi.org/10.1021/acs.cgd.6b00794. [Online]. Available: http://dx.doi.org/10.1021/acs.cgd.6b00794.

[16] D. Maes, M. A. Vorontsova, M. A. C. Potenza, T. Sanvito, M. Sleutel, M. Giglio, and P. G. Vekilov, "Do protein crystals nucleate within dense liquid clusters?", *Acta Crystallographica Section F Structural Biology Communications*, vol. 71, no. 7, pp. 815–822, 2015. DOI: 10.1107/s2053230x15008997.

[17] C. Haas and J. Drenth, "Understanding protein crystallization on the basis of the phase diagram", *Journal of Crystal Growth*, vol. 196, no. 2, pp. 388–394, 1999, ISSN: 0022-0248. DOI: http://dx.doi.org/10.1016/S0022-0248(98)00831-8. [Online]. Available: http://www.sciencedirect.com/science/article/pii/S0022024898008318.

[18] X. Sun, B. A. Garetz, and A. S. Myerson, "Polarization switching of crystal structure in the nonphotochemical laser-induced nucleation of supersaturated aqueous l-histidine", *Crystal Growth & Design*, vol. 8, no. 5, pp. 1720–1722, 2008. DOI: 10.1021/cg800028v. eprint: http://dx.doi.org/10.1021/cg800028v. [Online]. Available: http://dx.doi.org/10.1021/cg800028v.

[19] I. S. Lee, J. M. B. Evans, D. Erdemir, A. Y. Lee, B. A. Garetz, and A. S. Myerson, "Nonphotochemical laser induced nucleation of hen egg white lysozyme crystals", *Crystal Growth & Design*, vol. 8, no. 12, pp. 4255–4261, 2008. DOI: 10.1021/cg800696u. eprint: http://dx.doi.org/10.1021/cg800696u. [Online]. Available: http://dx.doi.org/10.1021/cg800696u.

[20] A. J. Alexander and P. J. Camp, "Single pulse, single crystal laser-induced nucleation of potassium chloride", *Crystal Growth & Design*, vol. 9, no. 2, pp. 958–963, 2009. DOI: 10.1021/cg8007415. eprint: http://dx.doi.org/10.1021/cg8007415. [Online]. Available: http://dx.doi.org/10.1021/cg8007415.

[21] W. Li, A. Ikni, P. Scouflaire, X. Shi, N. El Hassan, P. Gémeiner, J.-M. Gillet, and A. Spasojević-de Biré, "Non-photochemical laser-induced nucleation of sulfathiazole in a water/ethanol mixture", *Crystal Growth & Design*, vol. 16, no. 5, pp. 2514–2526, 2016. DOI: 10.1021/acs.cgd.5b01526. eprint: http://dx.doi.org/10.1021/acs.cgd.5b01526. [Online]. Available: http://dx.doi.org/10.1021/acs.cgd.5b01526.

[22] X. Sun, B. A. Garetz, and A. S. Myerson, "Supersaturation and polarization dependence of polymorph control in the nonphotochemical laser-induced nucleation (nplin) of aqueous glycine solutions", *Crystal Growth & Design*, vol. 6, no. 3, pp. 684–689, 2006. DOI: 10.1021/cg050460+. eprint: http://dx.doi.org/10.1021/cg050460+. [Online]. Available: http://dx.doi.org/10.1021/cg050460+.

[23] J. E. Aber, S. Arnold, B. A. Garetz, and A. S. Myerson, "Strong dc electric field applied to supersaturated aqueous glycine solution induces nucleation of the?polymorph", *Physical Review Letters*, vol. 94, no. 14, 2005. DOI: 10.1103/physrevlett.94.145503.

[24] B. C. Knott, M. F. Doherty, and B. Peters, "A simulation test of the optical kerr mechanism for laser-induced nucleation", *The Journal of Chemical Physics*, vol. 134, no. 15, p. 154 501, 2011. DOI: 10.1063/1.3574010. eprint: http://dx.doi.org/10.1063/1.3574010. [Online]. Available: http://dx.doi.org/10.1063/1.3574010.

[25] M. R. Ward and A. J. Alexander, "Nonphotochemical laser-induced nucleation of potassium halides: Effects of wavelength and temperature", *Crystal Growth & Design*, vol. 12, no. 9, pp. 4554–4561, 2012. DOI: 10.1021/cg300750c. eprint: http://dx.doi.org/10.1021/cg300750c. [Online]. Available: http://dx.doi.org/10.1021/cg300750c.

[26] D. Kashchiev, "On the influence of the electric field on nucleation kinetics", *Philosophical Magazine*, vol. 25, no. 2, pp. 459–470, 1972. DOI: 10.1080/14786437208226816. eprint: http://dx.doi.org/10.1080/14786437208226816. [Online]. Available: http://dx.doi.org/10.1080/14786437208226816.

[27] B. C. Knott, J. L. LaRue, A. M. Wodtke, M. F. Doherty, and B. Peters, "Communication: Bubbles, crystals, and laser-induced nucleation", *The Journal of Chemical Physics*, vol. 134, no. 17, p. 171 102, 2011. DOI: 10.1063/1.3582897. eprint: http://dx.doi.org/10.1063/1.3582897. [Online]. Available: http://dx.doi.org/10.1063/1.3582897.

[28] M. R. Ward, W. J. Jamieson, C. A. Leckey, and A. J. Alexander, "Laser-induced nucleation of carbon dioxide bubbles", *The Journal of Chemical Physics*, vol. 142, no. 14, p. 144 501, 2015. DOI: 10.1063/1.4917022. eprint: http://dx.doi.org/10.1063/1.4917022. [Online]. Available: http://dx.doi.org/10.1063/1.4917022.

[29] N. Mirsaleh-Kohan, A. Fischer, B. Graves, M. Bolorizadeh, D. Kondepudi, and R. N. Compton, "Laser shock wave induced crystallization", *Crystal Growth & Design*, vol. 17, no. 2, pp. 576–581, 2017. DOI: 10.1021/acs.cgd.6b01437. eprint: http://dx.doi.org/10.1021/acs.cgd.6b01437. [Online]. Available: http://dx.doi.org/10.1021/acs.cgd.6b01437.

[30] A. Myerson, *Handbook of industrial crystallization*. Elsevier, 2001.

[31] B.-h. Chai, J.-m. Zheng, Q. Zhao, and G. H. Pollack, "Spectroscopic studies of solutes in aqueous solution", *The Journal of Physical Chemistry A*, vol. 112, no. 11, pp. 2242–2247, 2008, PMID: 18298105. DOI: 10.1021/jp710105n. eprint: http://dx.doi.org/10.1021/jp710105n. [Online]. Available: http://dx.doi.org/10.1021/jp710105n.

[32] M. M. Pejovic, N. T. Nesic, M. M. Pejovic, D. V. Brajovic, and I. V. Denic, "Investigation of post-discharge processes in nitrogen at low pressure", *Physics of Plasmas*, vol. 19, no. 12, p. 123 512, 2012. DOI: 10.1063/1.4773026. eprint: http://dx.doi.org/10.1063/1.4773026. [Online]. Available: http://dx.doi.org/10.1063/1.4773026.

[33] S. Jiang and J. H. ter Horst, "Crystal nucleation rates from probability distributions of induction times", *Crystal Growth & Design*, vol. 11, no. 1, pp. 256–261, 2011. DOI: 10.1021/cg101213q. eprint: http://dx.doi.org/10.1021/cg101213q. [Online]. Available: http://dx.doi.org/10.1021/cg101213q.

[34] L. Wang, H. Feng, J. Peng, N. Dong, W. Li, and Y. Dong, "Solubility, metastable zone width, and nucleation kinetics of sodium dichromate dihydrate", *Journal of Chemical & Engineering Data*, vol. 60, no. 1, pp. 185–191, 2015. DOI: 10.1021/je5009069. eprint: http://dx.doi.org/10.1021/je5009069. [Online]. Available: http://dx.doi.org/10.1021/je5009069.

[35] K. Liang, G. White, D. Wilkinson, L. J. Ford, K. J. Roberts, and W. M. L. Wood, "An examination into the effect of stirrer material and agitation rate on the nucleation of l-glutamic acid batch crystallized from supersaturated aqueous solutions", *Crystal Growth & Design*, vol. 4, no. 5, pp. 1039–1044, 2004. DOI: 10.1021/cg034096v. eprint: http://dx.doi.org/10.1021/cg034096v. [Online]. Available: http://dx.doi.org/10.1021/cg034096v.

[36] M. W. Sigrist, "Laser generation of acoustic waves in liquids and gases", *Journal of Applied Physics*, vol. 60, no. 7, R83–R122, 1986. DOI: 10.1063/1.337089. eprint: http://dx.doi.org/10.1063/1.337089. [Online]. Available: http://dx.doi.org/10.1063/1.337089.

[37] Z. A. Schelly, J. Lang, and E. M. Eyring, "Relaxation of laser induced transient plasmas in liquids", *Monatshefte für Chemie / Chemical Monthly*, vol. 104, no. 6, pp. 1672–1677, Nov. 1973, ISSN: 1434-4475. DOI: 10.1007/BF00909653. [Online]. Available: https://doi.org/10.1007/BF00909653.

[38] A. B. Gojani, R. Bejtullahu, and S. Obayashi, "On two optomechanical effects of laser-induced electrostriction in dielectric liquids", *Japanese Journal of Applied Physics*, vol. 53, no. 9, p. 092 703, 2014. DOI: 10.7567/jjap.53.092703.

[39] E. Luscher, *Photoacoustic effect principles and applications*. Friedr. Vieweg & Sohn, 1984.

[40] C. K. N. PATEL and A. C. TAM, "Optical absorption coefficients of water", *Nature*, vol. 280, no. 5720, pp. 302–304, 1979. DOI: 10.1038/280302a0.

[41] A. C. Tam, C. K. N. Patel, and R. J. Kerl, "Measurement of small absorptions in liquids", *Opt. Lett.*, vol. 4, no. 3, pp. 81–83, Mar. 1979. DOI: 10.1364/OL.4.000081. [Online]. Available: http://ol.osa.org/abstract.cfm?URI=ol-4-3-81.

[42] P. Repond and M. W. Sigrist, "Photoacoustic spectroscopy on trace gases with continuously tunable co2 laser", *Appl. Opt.*, vol. 35, no. 21, pp. 4065–4085, Jul. 1996. DOI: 10.1364/AO.35.004065. [Online]. Available: http://ao.osa.org/abstract.cfm?URI=ao-35-21-4065.

[43] L. Zhang, W. She, N. Peng, and U. Leonhardt, "Experimental evidence for abraham pressure of light", *New Journal of Physics*, vol. 17, no. 5, p. 053 035, 2015. DOI: 10.1088/1367-2630/17/5/053035.

[44] S. E. Bialkowski, *Photothermal spectroscopy methods for chemical analysis*. John Wiley & Sons, 1996.

[45] A. Kumar, "Speed of sound in concentrated aqueous kcl solutions from 278.15 to 338.15 k", *Journal of Chemical & Engineering Data*, vol. 48, no. 2, pp. 388–391, 2003. DOI: 10.1021/je025605k. eprint: http://dx.doi.org/10.1021/je025605k. [Online]. Available: http://dx.doi.org/10.1021/je025605k.

[46] E. Kritchman, S. Shtrikman, and M. Slatkine, "Resonant optoacoustic cells for trace gas analysis*", *J. Opt. Soc. Am.*, vol. 68, no. 9, pp. 1257–1271, Sep. 1978. DOI: 10.1364/JOSA.68.001257. [Online]. Available: http://www.osapublishing.org/abstract.cfm?URI=josa-68-9-1257.

[47] S. Å. Ellingsen and I. Brevik, "Electrostrictive fluid pressure from a laser beam", *Physics of Fluids*, vol. 23, no. 9, p. 096 101, 2011. DOI: 10.1063/1.3638130. eprint: http://dx.doi.org/10.1063/1.3638130. [Online]. Available: http://dx.doi.org/10.1063/1.3638130.

[48] C. K. N. Patel and A. C. Tam, "Pulsed optoacoustic spectroscopy of condensed matter", *Rev. Mod. Phys.*, vol. 53, pp. 517–550, 3 Jul. 1981. DOI: 10.1103/RevModPhys.53.517. [Online]. Available: https://link.aps.org/doi/10.1103/RevModPhys.53.517.